Dual Diffusion effects on radiated Bio-convective Magnetohydrodynamics Powell-Eyring nanofluid flow along a vertical cone surface

P. Francis [1], P. Sambath [1,*], Ali J. Chamkha[2]

[1]Department of Mathematics, College of Engineering and Technology, SRM Institute of Science and Technology, Kattankulathur, Chennai, 603203, Tamil Nadu, India.

[2]Faculty of Engineering, Kuwait College of Science and Technology, Doha District, 35004, Kuwait.

*Corresponding author(s). E-mail(s): sampathp@srmist.edu.in;

Contributing authors: fp9469@srmist.edu.in; achamkha@yahoo.com;

Abstract

Non-Newtonian fluids play a crucial role in a wide range of applications involving the exchange of heat and mass. Nanoparticles are one of the key strategies for improving the performance of non-Newtonian fluids in terms of heat and mass transport. Nanoparticles, such as aluminum oxide and titanium dioxide, have exceptional thermal properties due to their high thermal conductivity. To thoroughly understand and optimize the behavior of non-Newtonian nanofluids over a cone surface, we employ numerical solution techniques. In the fluid flow, we also investigate the impacts of magnetohydrodynamics (MHD), thermal radiation ($0.5 \le R_d \le 1.5$), and dual diffusion ($0.4 \le N_b \le 0.8$ and $0.3 \le N_t \le 0.7$). In addition, we examine the impact of a fluid containing microorganisms on mass transmission and heat transfer. In order to convert the interconnected non-linear governing partial differential equations into non-linear ordinary differential equations, we utilize a similarity transformation. Then transform the non-linear ordinary differential equation (ODE) into a set of first-order ODEs. Subsequently, we utilize the Keller Box finite difference approach to obtain a solution for the non-linear ODE. The results of our study indicate that incorporating thermal radiation and MHD (magnetohydrodynamics) leads to increased rates of heat and mass transfer by enhancing the diffusion of microorganisms. We validate the reliability of our observations by comparing them to prior research.

Keywords: Bio-convection, Brownian motion, Eyring-Powell nanofluid, Thermal Radiation, Thermophoresis.

1. Introduction

There are many different sectors that make use of vertical cone-shaped equipment. Some of these industries include chemical extraction, food processing, brewing, beverage manufacturing, the metalworking industry for casting facilities, polymers, and textiles, among

others. These instruments frequently need to be cooled down quickly in order to enable repeated usage, which is an essential need for maintaining industrial operations. The production of high-quality, risk-free goods for people all over the world, including as food, medications, home cleaners, and personal hygiene products, is crucially dependent on vertical cone mixers, for instance. Through the design process, each type of vertical cone mixer is developed with certain industrial objectives in mind as it is being created. There is a perceptible improvement in grinding efficiency that occurs as a result of the utilisation of vertical cone mixers, which in turn causes the surface of the mixer to warm up on the cone. This heating takes place as a result of the rapid and thorough mixing of the mixture, which causes heat to be carried along the surface of the cone. This is the reason of the heating described above. Non-Newtonian fluids have been proven to perform better than conventional fluids when it comes to the pursuit of efficient cooling for these cones through our observations. In addition, we noticed that the use of nanofluids (H_2O / Al_2O_3 and H_2O / TiO_2) results in an increase in the effectiveness of heat transfer. We are going to concentrate on a particular kind of non-Newtonian fluid that is referred to as the Eyring-Powell fluid in this particular case. The purpose of this study is to evaluate the impact that microorganisms have on the processes of heat and mass movement. Subsequently, recommendations are made concerning the ways in which these effects can be minimised through the utilisation of magnetohydrodynamics (MHD) and thermal radiation.

Various researchers have examined the heat transfer of fluid flow with different geometrical characteristics, and the similarity approach [1,2] and finite difference method [3-5] have been used to solve the problem. Furthermore, several researchers have examined non-Newtonian fluid flow with various geometric designs [6-9]. In addition, investigators discovered that the MHD effects in fluid flow models amplify the heat [10-12]. Researchers Hayat et al. [13], Saleem et al. [14], and Khan et al. [15] looked into the mass and heat transfer of cone and plate surfaces under conditions of heat flow. Several researchers [16-19] have looked into the MHD mixed convection and natural convection of fluid flow problems with heat and mass flux conditions. The heat and mass transfer fluid flow problems with various boundary conditions and effects were quantitatively explored by Khan et al. [20-23]. Additionally, studies using nanoparticles have been conducted because it has been shown in a number of studies [24-27] that the inclusion of nanoparticles in a fluid improves mass transfer and heat transfer when compared to standard fluid flow models. Non-Newtonian fluid models have been added to the nanofluids, which are once again developed [28, 29]. Non-Newtonian fluid flow over various geometrical problems is studied by Waqas et al. [30], Balazadeh et al. [31], Layek et al. [32], and Oke [33], who solve the governing equations both analytically and numerically. Furthermore, Khan et al. [33-36] looked at the specific non-Newtonian-fluid (Eyring-Powell) flow problems with various geometries, in which there were additionally several enhanced impacts from mass transfer and heat. The cattaneo-Christov heat flux models for non-Newtonian nanofluid flow problems are studied and computationally addressed by Reddy et al. [37], Nazeer et al. [38], and Irfan et al. [39]. Simulation studies of the Powell-Eyring nanofluid and hybrid nanofluid fluid flow problems with the effects of MHD and heat radiation are conducted by Ibrahim [40], Oke [41], Patil et al. [42], and Hussain [43]. Numerous researchers looked at the various non-Newtonian nanofluids, including ferromagnetic powell-eyring fluid [44, 45], sutterby nanofluid [46, 47], and Williamson nanofluid [48-51]. This

study looked at the effects of non-Newtonian fluids on mass and heat transfer at various stress tensor levels. In several engineering applications, ferromagnetic polymer nanofluid flow has been studied by Tabrez et al. [52], Hussain et al. [53], and Khan et al. [54]. Numerous researchers have examined bio-convective non-Newtonian nanofluid flow problems in recent years, focusing on various geometries such as stretching surfaces [55-57], Riga surfaces [58], and channels [59] with different effects.

There is no research done that looks at how heat and mass transfer can be affected by the bio-convection flow of a Powel-Eyring nano fluid on vertical cone surface. As a result of this, we are going to look into the natural bio-convective flow of fluid that occurs over a cone in the vertical direction. In addition, we took into account the impacts of MHD, thermal radiation, Brownian motion, and the thermophoresis effect. At the moment, we are employing multiple nanoparticles (H_2O / Al_2O_3 and H_2O / TiO_2) in order to gain a more in-depth comprehension of heat and mass transfer.

The remainder of the paper is organized as follows: Section 2 contains the mathematical and physical models, as well as the governing equation and boundary conditions for the problem. Section 3 describes how to solve the governing equation using boundary conditions. Section 4 provides a summary and graphic explanation of the findings. In the subsequent Section 5, we provided some closing observations regarding the subject of the study. Finally the section 6 is the future direction and limitation of this study.

2. Mathematical representation of the model

Consider an incompressible, two-dimensional, and stable fluid that travels over a vertical cone. This fluid is subject to the effects of MHD, heat radiation and Thermophoresis and Brownian motion. The cone has a half-angle, shown by the symbol ω, and a radius, shown by the letter r. The y-axis is oriented perpendicular to the cone/plate surface, whereas the x-axis follows and deviates from the surface as it covers the component. The notations u and v are employed to denote the velocity components that are parallel to the x- and y-axes, respectively. The framework's mathematical structure is shown in Figure 1, which includes equations for concentration, momentum, energy, continuity, and micro-organisms density. The Powell-Eyring fluid's additional stress tensor can be expressed mathematically as [25,55]

$$\tau_{ij} = \frac{1}{\beta} sinh^{-1}\left(\frac{1}{d}\frac{\partial u_i}{\partial x_j}\right) + \mu\frac{\partial u_i}{\partial x_j}$$

The variable μ will be used to represent the dynamic viscosity, whereas β and d will be the characteristics associated with the Eyring–Powell fluid. Assuming,

$$sinh^{-1}\left(\frac{1}{d}\frac{\partial u_i}{\partial x_j}\right) = -\frac{1}{6}\left(\frac{1}{d}\frac{\partial u_i}{\partial x_j}\right)^3 + \frac{1}{d}\frac{\partial u_i}{\partial x_j}, \qquad |\frac{1}{d}\frac{\partial u_i}{\partial x_j}| \ll 1$$

These equations were obtained through the application of the Boussinesq approximation.

$$\frac{\partial(ru)}{\partial x}+\frac{\partial(rv)}{\partial y}=0 \tag{1}$$

$$\left(\rho_{nf}\right)\left(u\frac{\partial u}{\partial x}+v\frac{\partial u}{\partial y}\right)=\left(\mu_{nf}+\frac{1}{\beta d}-\frac{1}{2\beta d^{3}}\left(\frac{\partial u}{\partial y}\right)^{2}\right)\left(\frac{\partial^{2}u}{\partial y^{2}}\right)-\sigma_{1}(B_{0})^{2}u-\frac{\mu_{nf}}{k_{1}}u \tag{2}$$

$$+\left(\left(\rho\beta_{T}\right)_{nf}\left(T-T_{\infty}\right)+\left(\rho\beta_{C}\right)_{nf}\left(C-C_{\infty}\right)\right)gcos\omega+\left(\gamma\left(\rho\beta_{N}\right)_{nf}\Delta\rho\left(N-N_{\infty}\right)\right)gcos\omega$$

$$u\frac{\partial T}{\partial x}+v\frac{\partial T}{\partial y}-\frac{\tau}{\left(\rho c_{p}\right)_{nf}}\left[D_{B}\frac{\partial T}{\partial y}\frac{\partial C}{\partial y}+\frac{D_{T}}{T_{\infty}}\left(\frac{\partial T}{\partial y}\right)^{2}\right]=\alpha_{nf}\frac{\partial^{2}T}{\partial y^{2}}-\frac{1}{\left(\rho c_{p}\right)_{nf}}\left(\frac{\partial q_{r}}{\partial y}\right) \tag{3}$$

$$u\frac{\partial C}{\partial x}+v\frac{\partial C}{\partial y}-D_{B}\frac{\partial^{2}C}{\partial y^{2}}=\frac{D_{T}}{T_{\infty}}\frac{\partial^{2}T}{\partial y^{2}} \tag{4}$$

$$u\frac{\partial N}{\partial x}+v\frac{\partial N}{\partial y}-D_{n}\frac{\partial^{2}N}{\partial y^{2}}+\frac{bW_{c}}{(C_{w}-C_{\infty})}\frac{\partial}{\partial y}\left(N\frac{\partial C}{\partial y}\right)=0 \tag{5}$$

Conditions of the boundary are

$$\begin{aligned}&At\quad y=0:\ C=C_{w},\ u=0,\ T=T_{w},\ v=0,\ N=N_{w}\\&As\quad y\to\infty:\ C\to C_{\infty},\ T\to T_{\infty},\ N\to N_{\infty},\ u\to 0.\end{aligned} \tag{6}$$

The provided information includes expressions for the density ρ, thermal expansion coefficient β, heat capacity Cp and thermal conductivity k of nanofluids [Table 1].

$$\alpha_{nf}=\frac{k_{nf}}{\left(\rho c_{p}\right)_{nf}},\ \mu_{nf}\left(1-\phi\right)^{2.5}=\mu_{f},\ \rho_{nf}-\phi\rho_{s}=\left(1-\phi\right)\rho_{f},\ (\beta\rho)_{nf}-\phi(\beta\rho)_{s}=\left(1-\phi\right)(\beta\rho)_{f},$$

$$\left(\rho c_{p}\right)_{nf}-\phi(\rho c_{p})_{s}=\left(1-\phi\right)(\rho c_{p})_{f},\ \frac{k_{nf}}{k_{f}}=\left[\frac{k_{s}+(n-1)k_{f}-2\phi\left(k_{f}-k_{s}\right)}{(k_{s}+(n-1)k_{f}+\phi\left(k_{f}-k_{s}\right)}\right]$$

Through the utilization of the corresponding similarity transformations, the non-linear PDE that is regulating (1-6) can be transformed into a collection of non-linear ODEs. $\chi(\xi)=\frac{N-N_{\infty}}{N_{w}-N_{\infty}}$,

$$\Psi=\nu_{f}r(Gr)^{1/4}f(\xi),\quad \xi=\frac{y}{x}(Gr)^{1/4},\quad \varphi(\xi)=\frac{C-C_{\infty}}{C_{w}-C_{\infty}},\quad u=\frac{\nu_{f}}{x}(Gr)^{1/4}f'(\xi),\ \theta(\xi)=\frac{T-T_{\infty}}{T_{w}-T_{\infty}},$$

$$Gr=\frac{g\beta_{T}(T_{w}-T_{\infty})cos\omega x^{3}}{\nu_{f}^{2}},\ v=\frac{\nu_{f}}{4x}(Gr)^{1/2}\left[\xi f'(\xi)-7f(\xi)\right].$$

In the following, non-dimensional forms of momentum, temperature, concentration, and density of microorganisms are demonstrated through the utilization of similarity transformation.

$$\left(G_{1}+K-KN_{1}(f'')^{2}\right)f'''-G_{2}\left(\left(\frac{1}{2}\right)f'^{2}-\left(\frac{7}{4}\right)ff''\right)\quad-\Gamma\left(G_{1}+K-\frac{KN_{1}}{3}(f'')^{2}\right)f' \tag{7}$$

$$+G_{2}G_{3}\left(\theta+R_{b}\chi+N_{r}\varphi\right)-Mf'=0$$

$$\left(\frac{1}{\mathrm{P}_{r}}\right)G_{4}\left(\frac{k_{nf}}{k_{f}}+\left(\frac{4}{3}\right)R_{d}\right)\theta''+\left(\frac{7}{4}\right)f\theta'+G_{4}\left[N_{b}\theta'\varphi'+N_{t}\theta'^{2}\right]=0 \tag{8}$$

$$\left(\frac{1}{S_c}\right)\varphi''+\left(\frac{7}{4}\right)f\varphi'+\left(\frac{1}{S_c}\right)\frac{N_t}{N_b}\theta''=0 \tag{9}$$

$$\chi''-P_e\left(\chi'\varphi'\right)-\left(P_e\left(\chi+\sigma\right)\varphi''\right)=-\left(\frac{7}{4}\right)L_b f\chi' \tag{10}$$

The boundary conditions that correspond to them are

$$\begin{aligned} &At \quad \xi=0: f=0,\ f'=0,\theta=1,\varphi=1,\ \chi=1;\\ &As \quad \xi\to\infty: f'\to 0,\theta\to 0,\varphi\to 0,\ \chi\to 0. \end{aligned} \tag{11}$$

where, $K=\left(\frac{1}{\mu_f \mathrm{d}\beta}\right)$, $N_1=\frac{\nu_f^2\left(\mathrm{Gr}\right)^{\frac{3}{2}}}{2d^2x^4}$, $N_r=\frac{\beta_C(C_w-C_\infty)}{\beta_T(T_w-T_\infty)}$, $R_b=\frac{\beta_N(N_w-N_\infty)\Delta\rho\gamma}{\beta_T(T_w-T_\infty)}$, $S_c=\frac{\nu_f}{D_B}$,

$P_r=\frac{\nu_f}{\alpha_f}$, $L_b=\frac{\nu_f}{D_n}$, $\Gamma=\frac{(Gr)^{-1/2}x^2}{k_1}$, $M=\frac{\sigma_1.B_0^2(Gr)^{-1/2}x^2}{\mu_f}$, $P_e=\frac{bW_c}{D_n}$, $\sigma=\frac{N_\infty}{N_w-N_\infty}$,

$R_d=\frac{4\sigma^*.T^3}{k^*.k_f}$, $N_t=\frac{\tau D_T(T_w-T_\infty)}{(\mu c_p)_f T_\infty}$, $G_1=\left[\frac{1}{(1-\phi)^{2.5}}\right]$, $G_2=\left[1-\phi+\phi\left(\frac{\rho_s}{\rho_f}\right)\right]$, $N_b=\frac{\tau D_B(C_w-C_\infty)}{(\mu c_p)_f}$,

$G_3=\frac{\left[1-\phi+\phi\left(\frac{(\rho\beta)_s}{(\rho\beta)_f}\right)\right]}{\left[1-\phi+\phi\left(\frac{\rho_s}{\rho_f}\right)\right]}$, $G_4=\frac{1}{\left[1-\phi+\phi\left(\frac{(\rho c_p)_s}{(\rho c_p)_f}\right)\right]}$.

As illustrated below, the non-dimensional representations of the local skin friction coefficient C_f (Friction between the cone and non-Newtonian fluid), the local Nusselt factor N_u (Heat transfer rate), the local Sherwood factor S_h (Mass transfer rate), and the local microbial density value N_n (Micro-organisms diffusion rate) are presented.

$$N_u=-\frac{1}{(Gr)^{-1/4}}\left(\frac{k_{nf}}{k_f}+\frac{4}{3}Rd\right)\theta'(0),\ C_f=\frac{1}{(Gr)^{1/4}}(G_1+K)f''(0)-\frac{KN_1}{3}(f''(0))^3),$$

$$N_n=-\frac{1}{(Gr)^{-1/4}}\chi'(0),\ S_h=-\frac{1}{(Gr)^{-1/4}}\varphi'(0).$$

3. Computational Technique

In the realm of adaptable finite difference approaches for parabolic problems, the Keller-box technique is among the most notable instances. It is suitable for a system of non-linear coupled ODE. Before solving the equations (7-11), convert the non-linear coupled ODE system into the first order of coupled ODE. After that, apply the finite difference scheme appropriately. For linearization, apply Newton's method in the discretization equation. Finally, using the block elimination method to solve the linear equation system.

First, convert the equation (7-11) in first-order system of ODE by assuming

$$f'=l \tag{12}$$

$$l' = m \tag{13}$$
$$\theta' = o \tag{14}$$
$$\varphi' = p \tag{15}$$
$$\chi' = q \tag{16}$$
$$\left(G_1 + K - KN_1 m^2\right)m' - \frac{G_2}{2}l^2 - \Gamma\left(G_1 + K - \frac{KN_1 m^2}{3}\right)l + (7/4)A_2 fm - Ml + G_3 G_2(\theta + N_r\varphi + R_b\chi) = 0 \tag{17}$$
$$\left(\frac{k_{nf}}{k_f} + \frac{4}{3}Rd\right)o' + (7/4)\frac{P_r}{G_4}fo + P_r N_b op + P_r N_t o^2 = 0 \tag{18}$$
$$p' + (7/4)S_c fp + \frac{N_t}{N_b}o' = 0 \tag{19}$$
$$q' + (7/4)L_b fq - P_e pq - P_e(\chi + \sigma)p' = 0 \tag{20}$$

Therefore, the converted boundary conditions are

$$\begin{aligned} &At \quad \xi = 0: \ f = 0, l = 0, \theta = 1, \varphi = 1, \chi = 1; \\ &As \quad \xi \to \infty: l \to 0, \theta \to 0, \varphi \to 0, \chi \to 0. \end{aligned} \tag{21}$$

Now applying the finite difference scheme in above equation (12-21) and defining $\xi_0 = 0$, $\xi_j = \xi_{j-1} + h_j$, $\xi_j = \xi_\infty$ where, h_j is step size of the central difference approximation and $\Delta\xi = 1, 2, 3, \ldots J$.

$$f_j - f_{j-1} = h_j\left(\frac{l_j + l_{j-1}}{2}\right) \tag{22}$$
$$l_j - l_{j-1} = h_j\left(\frac{m_j + m_{j-1}}{2}\right) \tag{23}$$
$$\theta_j - \theta_{j-1} = h_j\left(\frac{o_j + o_{j-1}}{2}\right) \tag{24}$$
$$\varphi_j - \varphi_{j-1} = h_j\left(\frac{p_j + p_{j-1}}{2}\right) \tag{25}$$
$$\chi_j - \chi_{j-1} = h_j\left(\frac{q_j + q_{j-1}}{2}\right) \tag{26}$$
$$\left(A_1 + K - KN_1 m^2_{j-\frac{1}{2}}\right)\left(\frac{m_j - m_{j-1}}{h_j}\right) - \frac{G_2}{2}l^2_{j-\frac{1}{2}} + (7/4)G_2(fm)_{j-\frac{1}{2}} - \Gamma\left(G_1 + K - \frac{KN_1 m^2_{j-\frac{1}{2}}}{3}\right)l_{j-\frac{1}{2}} - Ml_{j-\frac{1}{2}} + G_3 G_2(\theta_{j-\frac{1}{2}} + N_r\varphi_{j-\frac{1}{2}} + R_b\chi_{j-\frac{1}{2}}) = 0 \tag{27}$$
$$\left(\frac{k_{nf}}{k_f} + \frac{4}{3}Rd\right)\left(\frac{o_j - o_{j-1}}{h_j}\right) + (7/4)\frac{P_r}{G_4}(fo)_{j-\frac{1}{2}} + P_r N_b(op)_{j-\frac{1}{2}} + P_r N_t o^2_{j-\frac{1}{2}} = 0 \tag{28}$$

$$\left(\frac{p_j - p_{j-1}}{h_j}\right) + (7/4)S_c(fp)_{j-\frac{1}{2}} + \frac{N_t}{N_b}\left(\frac{o_j - o_{j-1}}{h_j}\right) = 0 \tag{29}$$

$$\left(\frac{q_j - q_{j-1}}{h_j}\right) + (7/4)L_b(fq)_{j-\frac{1}{2}} - P_e(pq)_{j-\frac{1}{2}} - P_e(\chi_{j-\frac{1}{2}} + \sigma)\left(\frac{p_j - p_{j-1}}{h_j}\right) = 0 \tag{30}$$

The corresponding boundary conditions are

$$f_0 = 0, \quad l_0 = 0, \quad \theta_0 = 1, \quad \varphi_0 = 1, \quad \chi_0 = 1, \; l_J = 0, \quad \theta_J = 0, \quad \varphi_J = 0, \quad \chi_J = 0 \tag{31}$$

Now introduced the following expression to linearized the non-linear system of equation (22-31) by applying newton's method.

$$f_j^{k+1} = f_j^k + \delta f_j^k,\; l_j^{k+1} = l_j^k + \delta l_j^k,\; m_j^{k+1} = m_j^k + \delta m_j^k,\; \theta_j^{k+1} = \theta_j^k + \delta\theta_j^k,\; o_j^{k+1} = o_j^k + \delta o_j^k,$$

$$\varphi_j^{k+1} = \varphi_j^k + \delta\varphi_j^k,\; p_j^{k+1} = p_j^k + \delta p_j^k,\; \chi_j^{k+1} = \chi_j^k + \delta\chi_j^k,\; q_j^{k+1} = q_j^k + \delta q_j^k.$$

where $k = 0,1,2,3...$

we keeping the δf_j^k, δl_j^k, δm_j^k, $\delta\theta_j^k$, δo_j^k, $\delta\varphi_j^k$, δp_j^k, $\delta\chi_j^k$, δq_j^k terms in left side and rest of others terms in right side. This process gives the linear system of equation and for simplicity superscript k is dropped.

$$\delta f_j - \delta f_{j-1} + (l_j + l_{j-1})\left(\frac{-h_j}{2}\right) = (R_1)_{j-\frac{1}{2}} \tag{32}$$

$$\delta l_j - \delta l_{j-1} + (m_j + n_{j-1})\left(\frac{-h_j}{2}\right) = (R_2)_{j-\frac{1}{2}} \tag{33}$$

$$\delta\theta_j - \delta\theta_{j-1} + (o_j + o_{j-1})\left(\frac{-h_j}{2}\right) = (R_3)_{j-\frac{1}{2}} \tag{34}$$

$$\delta\varphi_j - \delta\varphi_{j-1} + (p_j + p_{j-1})\left(\frac{-h_j}{2}\right) = (R_4)_{j-\frac{1}{2}} \tag{35}$$

$$\delta\chi_j - \delta\chi_{j-1} + (q_j + q_{j-1})\left(\frac{-h_j}{2}\right) = (R_5)_{j-\frac{1}{2}} \tag{36}$$

$$\begin{aligned}&(A_1)\delta m_j + (A_2)\delta m_{j-1} + (A_3)\delta f_j + (A_4)\delta f_{j-1} + (A_5)\delta l_j + (A_6)\delta l_{j-1} + (A_7)\delta\theta_j \\ &+(A_8)\delta\theta_{j-1} + (A_9)\delta\varphi_j + (A_{10})\delta\varphi_{j-1} + (A_{11})\delta\chi_j + (A_{12})\delta\chi_{j-1} = (R_6)_{j-\frac{1}{2}}\end{aligned} \tag{37}$$

$$(B_1)\delta o_j + (B_2)\delta o_{j-1} + (B_3)\delta f_j + (B_4)\delta f_{j-1} + (B_5)\delta p_j + (B_6)\delta p_{j-1} = (R_7)_{j-\frac{1}{2}} \tag{38}$$

$$(C_1)\delta p_j + (C_2)\delta p_{j-1} + (C_3)\delta f_j + (C_4)\delta f_{j-1} + (C_5)\delta o_j + (C_6)\delta o_{j-1} = (R_8)_{j-\frac{1}{2}} \tag{39}$$

$$(D_1)\delta q_j + (D_2)\delta q_{j-1} + (D_3)\delta f_j + (D_4)\delta f_{j-1} + (D_5)\delta p_j + (D_6)\delta p_{j-1} = (R_9)_{j-\frac{1}{2}} \tag{40}$$

The boundary conditions are

$$\delta f_0 = 0,\; \delta l_0 = 0,\; \delta\theta_0 = 0,\; \delta\varphi_0 = 0,\; \delta\chi_0 = 0,\; \delta l_J = 0,\; \delta\theta_J = 0,\; \delta\varphi_J = 0,\; \delta\chi_J = 0 \tag{41}$$

Now we solve the system of linear equations (32-41) by block elimination method. A better convergence and a lower error rate are achieved by the issue as a result of the choice of initial guesses. The following are some of the preliminary assumptions that are made here.

$\chi_0(\xi) = e^{-\xi}, \quad f_{0'}(\xi) = 1 - e^{-\xi}, \quad \varphi_0(\xi) = e^{-\xi}, \quad \theta_0(\xi) = e^{-\xi}.$

It would appear that the step size $h_j = 0.006$ is an adequate convergence point for the technique that is currently being utilized. In addition, we insisted on adhering to the 10^{-6} error tolerance in each and every instance in order to arrive at a solution that exceeded expectations. It would appear that the values in Table 2 for each parameter change are in perfect agreement with one another, which is a strong indication that the validation of the approach is successful. These findings provide evidence that the Keller box method with finite differences is appropriate for our usage. In addition, we included the flowchart [Figure 2] for the Keller box approach in order to facilitate and enhance comprehension. Utilizing an AMD Ryzen 7 5800H system, we simulated the above model in MATLAB R2021a and presented it here.

4. Findings and Analysis

The heat and mass transfer that occurs during the flow of a bio-convective fluid is visually represented by this model. The parameter values of the model were established according to the description provided below. $R_b = 0.3$, $K = 0.4$, $N_1 = 2$, $\Gamma = 1$, $M = 1$, $P_r = 6.2$, $N_b = 0.5$, $N_t = 0.4$, $R_d = 0.6$, $S_c = 1$, $\sigma = 0.3$, $N_r = 0.5$, $P_e = 0.3$, $L_b = 0.7$. Unless explicitly stated otherwise, all values are constant. The lines in Figure (3-23) that share the same color and pattern represent Aluminum and Titanium, respectively.

4.1 Velocity Profile

Figure 3 demonstrates that an augmentation in the Powell-Eyring fluid component (K) leads to a decrease in the velocity distribution. Figure 4 shows that arise in the MHD factor (M) results in a drop in the profile of velocity. This is due to the perpendicular Lorentz force exerted on the fluid flow. The force mentioned leads to a boost in the amount of thickness of the boundary layer of momentum for the cone. Figures 5 and 6 demonstrate that an elevation in the buoyancy ratio factor (N_r) and biological convection Rayleigh value (R_b) results in an augmentation of the velocity distribution for cone shapes and this parameter leads to a higher level of momentum exchange within the fluid. Table 3 explains that the skin friction value increases when both the buoyancy ratio factor (N_r) and biological convection Rayleigh value (R_b) grow. On the other hand, when the Electromagnetic variable (M), fraction of volume (ϕ), and Powell-Eyring fluid variable (K) rises, the skin friction amount (C_f) falls. This decrease in C_f leads to a faster fluid flow across the cone. When the Electromagnetic variable (M) and porosity variable (Γ) are raised, titanium nanofluid shows the lowest skin friction value compared to other nanofluids such as Al_2O_3 and TiO_2.

4.2 Thermal Profile

As seen in Figure 7, an increase in the volume percentage (ϕ) leads to a greater temperature profile, demonstrating an improved heat exchange efficiency. The Powell-Eyring fluid variable (K) plays a crucial function and holds great importance, as seen in Figure 8. The figure demonstrates that greater quantities of K result in an enhanced thermal transfer efficiency. Figure 9 demonstrates that the heat transfer rate is enhanced by a boost in the MHD variable (M), as the

Lorentz force influences both the velocity and direction of the fluid. As shown in Figure 10, the most significant impact that porosity (Γ) has on heat transmission is the increased surface area that is available for heat exchange. Because of the permeable material's compact structure, it provides a large surface area for the fluid to interact with, which in turn makes it possible for the fluid to transfer heat at a faster rate. The impact of thermal radiation on the temperature profile is demonstrated in Figure 11, where an escalation in the thermal radiation parameter (R_d) leads to a heightened heat transfer rate. This phenomenon occurs as a result of fluids emitting heat radiation when their temperature exceeds that of their surroundings. This radiation consists of electromagnetic waves, which contribute to the rise in internal energy and heat. Figure 12 illustrates that an augmentation in the Brownian motion parameter (N_b) leads to a minimize in the thickness of the boundary layer of thermal energy. In small-scale systems, the random movement of particles caused by Brownian motion leads to an increase in their collision rate. This, in turn, enhances the efficiency of heat transmission between the particles and the surrounding fluid. Therefore, Brownian motion plays a vital role in improving heat transfer at the micro- and nanoscales. Figure 13 provides a clear illustration of the rise in the thermophoresis parameter (N_t) and presents the measurement of the thin thermal boundary layer thickness. The text provides a clear explanation for the observed increase in the rate of heat transmission. The thermophoresis parameter controls the movement of particles, resulting in an enhanced heat transmission. Figure 14 reveals the temperature profile of different Prandtl numbers (P_r), which are significant in the fields of fluid mechanics and heat transfer since they represent the relative rates of momentum and thermal diffusion. According to Table 4, increasing the volume percentage (ϕ), thermal radiation (R_d), Brownian motion (N_b), and Thermophoresis (N_t) factors leads to higher heat transfer rates for aluminum compared to titanium. In general, these figures provide significant information on how to maximize the efficiency of heat transfer in different situations.

4.3 Profile of Concentration

Figure 15 illustrates that a boost in the percentage of volume (ϕ) results in an elevated concentration and rate of diffusion. This is attributed to the existence of nanoparticles, which impede molecular mobility and influence transport parameters. An illustration of the influence of magnetohydrodynamics (MHD) and an increase in the MHD factor (M) on the quantity of thickness of the concentration boundary layer and the efficient rate of mass movement is presented in Figure 16. The MHD has the capability to increase fluid contact, which contributes to an improvement in the manner in which mass is transmitted. Figures 17 and 18 illustrate the impact of Brownian motion as well as thermophoresis on the concentration distribution. As stated in the temperature profile for these two phenomena, they are causing an increase in thermal transfer rates. Similarly, when the Brownian motion (N_b) and thermophoresis (N_t) parameters are increased, the resulting narrow concentration boundary layer becomes thicker. The text provides a detailed explanation of how Brownian motion and thermophoresis processes contribute to the enhancement of mass exchange rates. Figure 19 exhibits concentration profiles of different Schmidt values, which quantify the relative rates of both momentum and mass transfer in a fluid. The Sherwood value indicates the effectiveness of the transfer of mass. The data presented in Table 5 demonstrates that an increase in the Brownian motion factor (N_b) and Schmidt values (S_c) leads

to an increase in the local Sherwood number ($-\varphi'(0)$). On the other hand, when the volume fraction (ϕ), Powell-Eyring fluid variable (K), and thermophoresis factor (N_t) increase, the Sherwood value ($-\varphi'(0)$) decreases.

4.4 Density of Micro-organisms Profile

Figure 20 shows that when magnetohydrodynamics (M) is applied to a fluid containing microorganisms, the thickness of the diffusion boundary layer surrounding the microorganisms decreases and their diffusion rate increases. Microorganisms are made easier to mix and disperse when a magnetic field and a flowing fluid contact, producing electric currents that cause MHD. It is depicted in Figure 21 that the influence of heat radiation (R_d) on the outside temperature and density of a liquid that contains microbes is shown. The temperature-induced densities transition causes warmer, thinner fluid to rise and denser, more relaxed fluid to sink. These fluxes influence the dispersion of chemicals in the vicinity of microorganisms. Figure 22 illustrates that an increase in the biological convection Peclet value (P_e) leads to an improvement in mixing of liquids because microorganisms are able to move around the medium. Figure 23 demonstrates the influence of an elevated Lewis number (L_b) on the stability of biological convection and the formation of patterns. When there is a rise in the Lewis factor (L_b), thermal propagation takes precedence over mass transmission. This change in the equilibrium of the biological processes that are responsible for diffusion has an effect on the buoyant forces that are responsible for driving biological convection, which ultimately results in a fall in the reliability of the distribution patterns. The data presented in Table 6 reveals that the average number of local microorganisms ($-\chi'(0)$) decreases as the Eyring-Powell fluid factor (K) and the volume percentage for the cone-shaped areas increase. On the other hand, an increase in the number of the local microbial densities ($-\chi'(0)$) is a consequence of a greater amount of the heat radiation factor (R_d), the biological convection Lewis value (L_b), and the biological convection Peclet variable (P_e).

5. Conclusion

The primary objective of this research was to investigate the flow properties of a bio-convective nanofluid that exhibited non-Newtonian behavioural patterns. Particularly, the Eyring-Powell fluid framework was utilised for this investigation. An investigation into the flow was carried out in respect to an upright cone. Additionally, the effects of thermal radiation, magnetohydrodynamics (MHD), thermophoresis, and Brownian motion were taken into consideration in this inquiry. The goal of the present study was to acquire a more thorough understanding of the mechanisms that are connected with heat and mass transmission. To gain a thorough understanding of the model, we looked at a variety of physical aspects of application data analysis. When we compared the results to those of earlier studies, there was noticeable agreement. The study's observations led to the following important conclusions:

- When increasing the Magnetohydrodynamic (MHD) parameter
    - The heat and mass transfer rate increased.
    - The micro-organisms diffusion rate increased.

- The flow velocity decreased.

❖ When increasing Porosity (Γ) and thermal radiation (R_d) parameter

- The heat transfer rate increased.

❖ When increasing Eyring-Powell fluid (K) parameter

- The flow velocity decreased.
- The heat transfer rate increased.

❖ When increasing volume fraction (ϕ) of nanoparticle, thermophoresis (N_t), and Brownian motion (N_b)

- The heat and mass transfer rate increased.

6. The future path

Future studies on the fluctuations of heat and mass transfer in non-Newtonian fluids with microorganisms under unstable conditions might be carried out in greater detail. One of the limitations of the current model is that it is unable to account for combined convection in an environment that is characterized by fluid flow.

Author Contributions

The study's concept and design were developed by PF, PS, and AJC. PF searched for relevant material and wrote the paper. Data processing and interpretation were tasks performed by PS and AJC. PS oversaw the entire research project. This final manuscript has been read and approved by all authors.

Data availability This article includes the datasets used to draw its results.

Declarations

Conflicts of interest The authors declare no conflict of interest.

Terminology

u , v	Velocity component (ms^{-2})
x , y	Coordinate (m)
g	Acceleration due to gravity
r	Radius of the cone
d	Physical Eyring-Powell fluid parameter
T	Temperature (K)
C	Concentration $(mol.m^3)$
N	Density of micro-organisms
Cp_{nf} , Cp_f	Specific heat $(Jkg^{-1}K^{-1})$
N_b	Brownian motion parameter
D_B	Mass diffusivity (m^2s^{-1})
B_0^2	Magnetic parameter
N_t	Thermophoresis parameter
b	Chemotaxis constant

W_c	The maximum cell swimming speed $(m^2 s^{-1})$
D_n	Diffusivity of micro-organisms (ms^{-1})
K	Dimensionless Eyring-Powell parameter
N_1	Non-Newtonian fluid parameter
N_r	Buoyancy ratio parameter
R_b	Bio-convection Rayleigh number
M	Dimensionless magnetic parameter
k_1	Porosity parameter
f	Dimensionless velocity function
S_c	Schmidt number
P_r	Prandtl number
L_b	Bio-convection Lewis number
P_e	Bio-convection Peclet number

Greek symbols

ω	Half angle of vertical cone
ρ_{nf} , ρ_f , ρ_s	Density (kgm^{-3})
β	Characteristics parameter of the Eyring-Powell fluid
μ_{nf} , μ_f , μ_s	Dynamic viscosity $(kgm^{-1}s^{-1})$
β_T , β_C , β_N	Volumetric expansion
γ	The mean quantity of microbes
α_{nf}	Thermal diffusivity of nanofluid $(m^2 s)$
ϕ	Volume fraction of nanofluid
ψ	Stream function
σ_1	Electrical conductivity (sm^{-1})
Γ	Dimensionless porosity constant
ξ	Dimensionless boundary layer coordinate
ν_{nf} , ν_f	Kinematic viscosity $(m^2 s^{-1})$
θ	Temperature function(non-dimensional)
φ	Concentration function(non-dimensional)
χ	Micro-organisms density function(non-dimensional)
σ	Bio-convection constant

Subscripts

f	Condition of base fluid
nf	Condition of nanofluid
s	Condition of nanoparticle
w	Condition of wall
∞	Condition of ambient

References

1. Hansen, A. and Na, T. “Similarity solutions of laminar, incompressible boundary layer equations of non-Newtonian fluids”, *ASME. J. Basic Eng.,* 90(1), pp.71-74 (1968). https://doi.org/10.1115/1.3605067
2. Lin, F. “Laminar free convection from a vertical cone with uniform surface heat flux”, *Letters Heat Mass Transfer*, **3**, pp. 49–58 (1976).
3. Pop, I. and Watanabe, T. “Free convection with uniform suction or injection from a vertical cone for constant wall heat flux”, *International communications in heat and mass transfer*, **19**(2), pp. 275–283 (1992). https://doi.org/10.1016/0735-1933(92)90038-J
4. Tripathi, R., Sau, A., and Nath, G. “Laminar free convection flow over a cone embedded in a stratified medium”, *Mechanics research communications*, **21**(3), pp. 289–296 (1994). http://eprints.iisc.ac.in/id/eprint/7755
5. Hossain, M. and Paul, S. “Free convection from a vertical permeable circular cone with non-uniform surface temperature”, *Acta mechanica*, **151**(1), pp. 103–114 (2001). https://doi.org/10.1007/BF01272528
6. Shima, A. and Tsujino, T. “The effect of polymer concentration on the bubble behaviour and impulse pressure”, *Chemical Engineering Science*, **36**(5), pp. 931–935 (1981). https://doi.org/10.1016/0009-2509(81)85047-6
7. Hartnett, J. P. and Kwack, E. “Prediction of friction and heat transfer for viscoelastic fluids in turbulent pipe flow”, *International journal of thermophysics*, **7**(1), pp. 53–63 (1986). https://doi.org/10.1007/BF00503798
8. Sirohi, V., Timol, M., and Kalthia, N. “Powell-Eyring model flow near an accelerated plate”, *Fluid dynamics research*, **2**(3), p. 193 (1987). https://doi.org/10.1016/0169-5983(87)90029-3
9. Shima, A., Rajvanshi, S. C., and Tsujino, T. “Study of nonlinear oscillations of bubbles in Powell–Eyring fluids”, *The Journal of the Acoustical Society of America*, **77**(5), pp. 1702–1709 (1985). https://doi.org/10.1121/1.391917
10. Fuchs, M. and Seregin, G. “Some remarks on non-Newtonian fluids including nonconvex perturbations of the Bingham and Powell–Eyring model for viscoplastic fluids”, *Mathematical Models and Methods in Applied Sciences*, **7**(3), pp. 405–433 (1997). https://doi.org/10.1142/S0218202597000232
11. Prasad, D. K., Chaitanya, G. K., and Raju, R. S. “Simultaneous Effects Thermal Diffusion and Diffusion Thermo on MHD Non-Newtonian Casson Fluid Flow Along A Vertically Inclined Plate in Presence of Free Convection and Joules Dissipation” (2006).
12. Mahmoud, M. A. and Megahed, A. M. “MHD flow and heat transfer in a non-Newtonian liquid film over an unsteady stretching sheet with variable fluid properties”, *Canadian Journal of Physics*, **87**(10), pp. 1065–1071 (2009). https://doi.org/10.1139/P09-066
13. Hayat, T., Awais, M., Nawaz, M., et al. “Mixed convection three-dimensional flow with Hall and ion-slip effects”, *Int. J. Nonlinear Sci. Numer. Simul*., **14**(3–4), pp. 167–177 (2013).

14. Saleem, S., Nadeem, S., and Haq, R. U. "Buoyancy and metallic particle effects on an unsteady water-based fluid flow along a vertically rotating cone", *The European Physical Journal Plus*, **129**(10), pp. 1–8 (2014). https://doi.org/10.1140/epjp/i2014-14213-1
15. Khan, N. A. and Sultan, F. "On the double diffusive convection flow of Eyring-Powell fluid due to cone through a porous medium with Soret and Dufour effects", *AIP advances*, **5**(5), p. 057140 (2015). https://doi.org/10.1063/1.4921488
16. Jayachandra Babu, M., Sandeep, N., and Raju, C. S. "Heat and mass transfer in MHD Eyring-Powell nanofluid flow due to cone in porous medium", *International Journal of Engineering Research in Africa*, **19**, pp. 57–74 (2016). https://doi.org/10.4028/www.scientific.net/JERA.19.57
17. Raju, C. and Sandeep, N. "Heat and mass transfer in MHD non-Newtonian bio-convection flow over a rotating cone/plate with cross diffusion", *Journal of molecular liquids*, **215**, pp. 115–126 (2016). https://doi.org/10.1016/j.molliq.2015.12.058
18. Khan, I., Khan, M., Malik, M., et al. "Mixed convection flow of Eyring-Powell nanofluid over a cone and plate with chemical reactive species", *Results in physics*, **7**, pp. 3716–3722 (2017). https://doi.org/10.1016/j.rinp.2017.08.042
19. Rehman, K. U., Saba, N. U., Malik, et al. "Encountering heat and mass transfer mechanisms simultaneously in Powell-Erying fluid through Lie symmetry approach", *Case studies in thermal engineering*, **10**, pp. 541–549 (2017). https://doi.org/10.1016/j.csite.2017.10.011
20. Khan, W., Ahmad, A., Anjum, N., et al. "Impact of nanoparticles and radiation phenomenon on viscoelastic fluid", *International Journal of Modern Physics B*, **36**(5), p. 2250049 (2022). https://doi.org/10.1142/S0217979222500497
21. Khan, W., Anjum, N., Waqas, M., et al. "Impact of stratification phenomena on a nonlinear radiative flow of sutterby nanofluid", *Journal of Materials Research and Technology*, **15**, pp. 306–314 (2021). https://doi.org/10.1016/j.jmrt.2021.08.011
22. Khan, W., Sun, H., Shahzad, M., et al. "Importance of heat generation in chemically reactive flow subjected to convectively heated surface", *Indian Journal of Physics*, **95**, pp. 89–97 (2021). https://doi.org/10.1007/s12648-019-01678-2
23. Khan, W. A., Waqas, M., Kadry, S., et al. "On the evaluation of stratification-based entropy optimized hydromagnetic flow featuring dissipation aspect and Robin conditions", *Computer Methods and Programs in Biomedicine*, **190**, p. 105347 (2020). https://doi.org/10.1016/j.cmpb.2020.105347
24. Gorla, R. S. R., El-Kabeir, S., and Rashad, A. "Boundary-layer heat transfer from a stretching circular cylinder in a nanofluid", *Journal of thermophysics and heat transfer*, **25**(1), pp. 183–186 (2011). https://doi.org/10.2514/1.51615
25. Babu, B. H., Srinivasa Rao, P., Reddy, M. G., et al. "Modeling of cattaneo-christov heat and mass flux on non-newtonian hydromagnetic fluid with variable thermal and solutal properties", *Proceedings of the Institution of Mechanical Engineers, Part E: Journal of Process Mechanical Engineering*, p. 09544089211046081 (2021). https://doi.org/10.1177/09544089211046081
26. Qaiser, D., Zheng, Z., and Khan, M. R. "Numerical assessment of mixed convection flow of Walters-B nanofluid over a stretching surface with Newtonian heating and mass

transfer", *Thermal Science and Engineering Progress*, **22**, p. 100801 (2021). https://doi.org/10.1016/j.tsep.2020.100801
27. Li, Y.-X., Hamid, A., Khan, M. I., et al. "Dual branch solutions (multi-solutions) for nonlinear radiative Falkner–Skan flow of Maxwell nanomaterials with heat and mass transfer over a static/moving wedge", *International Journal of Modern Physics C*, **32**(10), p. 2150130 (2021). https://doi.org/10.1142/S0129183121501308
28. Eldabe, N. T., Elbashbeshy, E. M., Hasanin, W. S., et al. "Effects of Heat and Mass Transfer on Unsteady MHD Free Convection Flow of Non-Newtonian Powell-Eyring Model Through a Porous Medium Near a Moving Vertical Plate in the Presence of Chemical Reaction and Heat Generation".
29. Zaman, H., Shah, M. A., and Ibrahim, M. "Unsteady incompressible Couette flow problem for the Eyring-Powell model with porous walls", *American Journal of Computational Mathematics*, **2013** (2013). https://doi.org/10.4236/ajcm.2013.34041
30. Waqas, M., Khan, M. I., Hayat, T., et al. "On Cattaneo–Christov double diffusion impact for temperature-dependent conductivity of Powell–Eyring liquid", *Chinese Journal of physics*, **55**(3), pp. 729–737 (2017). https://doi.org/10.1016/j.cjph.2017.02.003
31. Balazadeh, N., Sheikholeslami, M., Ganji, D. D., et al. "Semi analytical analysis for transient Eyring-Powell squeezing flow in a stretching channel due to magnetic field using DTM", *Journal of Molecular Liquids*, **260**, pp. 30–36 (2018). https://doi.org/10.1016/j.molliq.2018.03.066
32. Layek, G., Mandal, B., and Bhattacharyya, K. "Dufour and soret effects on unsteady heat and mass transfer for powell-eyring fluid flow over an expanding permeable sheet", *Journal of Applied and Computational Mechanics*, **6**(4), pp. 985–998 (2020). https://doi.org/10.22055/JACM.2019.30018.1661
33. Oke, A. "Coriolis effects on MHD flow of MEP fluid over a non-uniform surface in the presence of thermal radiation", *International Communications in Heat and Mass Transfer*, **129**, p. 105695 (2021). https://doi.org/10.1016/j.icheatmasstransfer.2021.105695
34. Khan, S. U., Waqas, H., Muhammad, T., et al. "Simultaneous effects of bioconvection and velocity slip in three-dimensional flow of Eyring-Powell nanofluid with Arrhenius activation energy and binary chemical reaction", *International Communications in Heat and Mass Transfer*, **117**, p. 104738 (2020). https://doi.org/10.1016/j.icheatmasstransfer.2020.104738
35. Khan, B. M. H., Gaffar, S. A., Beg, O. A., et al. "Computation of Eyring-Powell micropolar convective boundary layer flow from an inverted non-isothermal cone: thermal polymer coating simulation", *Computational Thermal Sciences: An International Journal*, **12**(4) (2020). https://doi.org/10.1615/ComputThermalScien.2020033860
36. Khan, N. M., Bacha, H. B., Pan, K., et al. "Nonlinear Eyring–Powell bioconvective nanofluid flow over a vertical plate with temperature dependent viscosity and surface suction", *International Communications in Heat and Mass Transfer*, **128**, p. 105602 (2021). https://doi.org/10.1016/j.icheatmasstransfer.2021.105602
37. Reddy, P. S. and Sreedevi, P. "Effect of Cattaneo–Christov heat flux on heat and mass transfer characteristics of Maxwell hybrid nanofluid flow over stretching/shrinking sheet", *Physica Scripta*, **96**(12), p. 125237 (2021). https://doi.org/10.1088/1402-4896/ac2f7d

38. Nazeer, M., Khan, M. I., Khan, S. U., et al. “Assessment of heat and mass transfer characteristics in Poiseuille flow of non-Newtonian nanofluid in a porous channel with convectively heated lower wall”, *Chinese Journal of Physics*, **77**, pp. 1065–1079 (2022). https://doi.org/10.1016/j.cjph.2021.10.021
39. Irfan, M., Khan, W., Pasha, A. A., et al. “Significance of non-Fourier heat flux on ferromagnetic Powell-Eyring fluid subject to cubic autocatalysis kind of chemical reaction”, *International Communications in Heat and Mass Transfer*, **138**, p. 106374 (2022). https://doi.org/10.1016/j.icheatmasstransfer.2022.106374
40. Ibrahim, M. “Concentration-dependent viscosity effect on magnetonano peristaltic flow of Powell-Eyring fluid in a divergent-convergent channel”, *International Communications in Heat and Mass Transfer*, **134**, p. 105987 (2022). https://doi.org/10.1016/j.icheatmasstransfer.2022.105987
41. Oke, A. “Theoretical analysis of modified eyring powell fluid flow”, *Journal of the Taiwan Institute of Chemical Engineers*, **132**, p. 104152 (2022). https://doi.org/10.1016/j.jtice.2021.11.019
42. Patil, P. and Kulkarni, M. “MHD quadratic mixed convective Eyring-Powell nanofluid flow with multiple diffusions”, *Chinese Journal of Physics*, **77**, pp. 393–410 (2022). https://doi.org/10.1016/j.cjph.2022.03.007
43. Hussain, M., Ranjha, Q. A., Anwar, M. S., et al. “Eyring-Powell model flow near a convectively heated porous wedge with chemical reaction effects”, *Journal of the Taiwan Institute of Chemical Engineers*, **139**, p. 104510 (2022). https://doi.org/10.1016/j.jtice.2022.104510
44. Irfan, M., Khan, W., Pasha, A. A., et al. “Significance of non-Fourier heat flux on ferromagnetic Powell-Eyring fluid subject to cubic autocatalysis kind of chemical reaction”, *International Communications in Heat and Mass Transfer*, **138**, p. 106374 (2022). https://doi.org/10.1016/j.icheatmasstransfer.2022.106374
45. Hussain, M., Ali, A., Ranjha, Q. A., et al. “Radiative magneto-cross Eyring-Powell flow with activation energy past porous stretching wedge considering suction/injection and ohmic heating effect”, *Numerical Heat Transfer, Part B: Fundamentals*, pp. 1–16 (2023). https://doi.org/10.1080/10407790.2023.2257383
46. Azeem Khan, W. “Impact of time-dependent heat and mass transfer phenomenon for magnetized Sutterby nanofluid flow”, *Waves in random and complex media*, pp. 1–15 (2022). https://doi.org/10.1080/17455030.2022.2140857
47. Khan, W., Arshad, Z., Hobiny, A., et al. “Impact of magnetized radiative flow of sutterby nanofluid subjected to convectively heated wedge”, *International Journal of Modern Physics B*, **36**(16), p. 2250079 (2022). https://doi.org/10.1142/S0217979222500795
48. Khan, W. A. “Significance of magnetized Williamson nanofluid flow for ferromagnetic nanoparticles”, *Waves in Random and Complex Media*, pp. 1–20 (2023). https://doi.org/10.1080/17455030.2023.2207390
49. Khan, W. A., Waqas, M., Chammam, W., et al. “Evaluating the characteristics of magnetic dipole for shear-thinning Williamson nanofluid with thermal radiation”, *Computer Methods and Programs in Biomedicine*, **191**, p. 105396 (2020). https://doi.org/10.1016/j.cmpb.2020.105396

50. Saleem, M. and Hussain, M. “Dual solutions of Williamson-Casson fluid over a heated exponentially shrinking surface with stability analysis: A novel Catteneo-Christov heat flux model combination”, *Numerical Heat Transfer, Part A: Applications*, pp. 1–23 (2023). https://doi.org/10.1080/10407782.2023.2252583
51. Saleem, M., Hussain, M., and Inc, M. “Significance of Darcy–Forchheimer law and magnetic field on the comparison of Williamson–Casson fluid subject to an exponential stretching sheet”, *International Journal of Modern Physics B*, **37**(27), p. 2350315 (2023). https://doi.org/10.1142/S0217979223503150
52. Tabrez, M. and Azeem Khan, W. “Exploring physical aspects of viscous dissipation and magnetic dipole for ferromagnetic polymer nanofluid flow”, *Waves in random and complex media*, pp. 1–20 (2022). https://doi.org/10.1080/17455030.2022.2135794
53. Hussain, Z. and Azeem Khan, W. “Impact of thermal-solutal stratifications and activation energy aspects on time-dependent polymer nanoliquid”, *Waves in random and complex media*, pp. 1–11 (2022). https://doi.org/10.1080/17455030.2022.2128229
54. Khan, W., Ali, M., Irfan, M., et al. “A rheological analysis of nanofluid subjected to melting heat transport characteristics”, *Applied Nanoscience*, **10**, pp. 3161–3170 (2020). https://doi.org/10.1007/s13204-019-01067-5
55. Mahdy, A. “Unsteady Mixed Bioconvection Flow of Eyring–Powell Nanofluid with Motile Gyrotactic Microorganisms Past Stretching Surface”, *Bio-NanoScience*, **11**(2), pp. 295–305 (2021). https://doi.org/10.1007/s12668-021-00857-y
56. Anjum, N., Khan, W., Hobiny, A., et al. “Numerical analysis for thermal performance of modified Eyring Powell nanofluid flow subject to activation energy and bioconvection dynamic”, *Case Studies in Thermal Engineering*, **39**, p. 102427 (2022). https://doi.org/10.1016/j.csite.2022.102427
57. Waqas, M., Khan, W., Pasha, A. A., et al. “Dynamics of bioconvective Casson nanoliquid from a moving surface capturing gyrotactic microorganisms, magnetohydrodynamics and stratifications”, *Thermal Science and Engineering Progress*, **36**, p. 101492 (2022). https://doi.org/10.1016/j.tsep.2022.101492
58. Khan, M. I., Shah, F., Khan, S. U., et al. “Heat and mass transfer analysis for bioconvective flow of Eyring Powell nanofluid over a Riga surface with nonlinear thermal features”, *Numerical Methods for Partial Differential Equations*, **38**(4), pp. 777–793 (2022). https://doi.org/10.1002/num.22696
59. Akbar, Y. and Huang, S. “Enhanced thermal effectiveness for electrokinetically driven peristaltic flow of motile gyrotactic microorganisms in a thermally radiative Powell Eyring nanofluid flow with mass transfer”, *Chemical Physics Letters*, **808**, p. 140120 (2022). https://doi.org/10.1016/j.cplett.2022.140120

Biographies

P. Francis is a Ph.D. research scholar in the Department of Mathematics at SRM Institute of Science and Technology, located in Kattangulathur, Chengalpattu, Tamil Nadu, India. He completed his M.Sc. in Mathematics at Bishop Heber College in Trichy, Tamil Nadu, India. His

current research interests include the numerical investigation of heat and mass transfer, nanofluid flow, and non-Newtonian fluid flow. He has published three research articles in reputed journals.

Dr. P. Sambath is an Associate professor in the Department of Mathematics at SRM Institute of Science and Technology, Kattankulathur, Tamil Nadu, India. He earned his Ph.D. in Computational Fluid Dynamics from SRM Institute of Science and Technology in 2017, and holds an M.Phil. and a P.G.D.C.A. from Alagappa University, along with an M.Sc. and B.Sc. from Madurai Kamaraj University. His research interests include unsteady heat and mass transfer, heat and mass flux, free convection flow, MHD flow, nanofluid flow, and bio-convection. Dr. Sambath has published 30 research articles in reputed journals. He is a life member of ISTE (The Indian Society for Technical Education, Membership No: LM 137283), ISCA (Indian Science Congress Association, Membership No: L30322), and IAENG (International Association for Engineers, Membership No: 223012).

Ali J. Chamkha is a Distinguished Professor of Mechanical Engineering and Dean of Engineering at Kuwait College of Science and Technology. He earned his Ph.D. in Mechanical Engineering from Tennessee Technological University, USA, in 1989. His research interests include multiphase fluid-particle dynamics, nanofluids dynamics, fluid flow in porous media, heat and mass transfer, magnetohydrodynamics and fluid-particle separation. He is currently the Editor-in-Chief for the Journal of Nanofluids and has served as an Editor, Associate Editor or a member of the editorial board for many journals such as ASME Journal of Thermal Science and Engineering Applications, ASME Journal of Nuclear Engineering and Radiation Science, International Journal of Numerical Method for Heat and Fluid Flow, Journal of Thermal Analysis and Calorimetry, Thermal Science journal, Scientia Iranica, Special Topics & Reviews in Porous Media, Journal of Porous Media, Journal of Thermal Engineering, Recent Patents on Mechanical Engineering, Journal of Applied Fluid Mechanics, International Journal of Fluids and Thermal Sciences, Journal of Heat and Mass Transfer Research, International Journal for Microscale and Nanoscale Thermal and Fluid Transport Phenomena, International Journal of Industrial Mathematics and many others. He has authored and co-authored over 1250 publications in archival international journals and conferences. His current h-index is 139 and total citations is 60,755. Professor Chamkha was included in the World's Top 2% Scientists 2020, 2021, 2022 and 2023 lists (by Stanford University) with a Global Rank #21, #20, #23 and #14 out of a total of 92,645, 109,724, 121,447 and 133,525, respectively and Rank #1 at the Arab World level in Mechanical Engineering and Transports category for all these years..

List of Figuers:

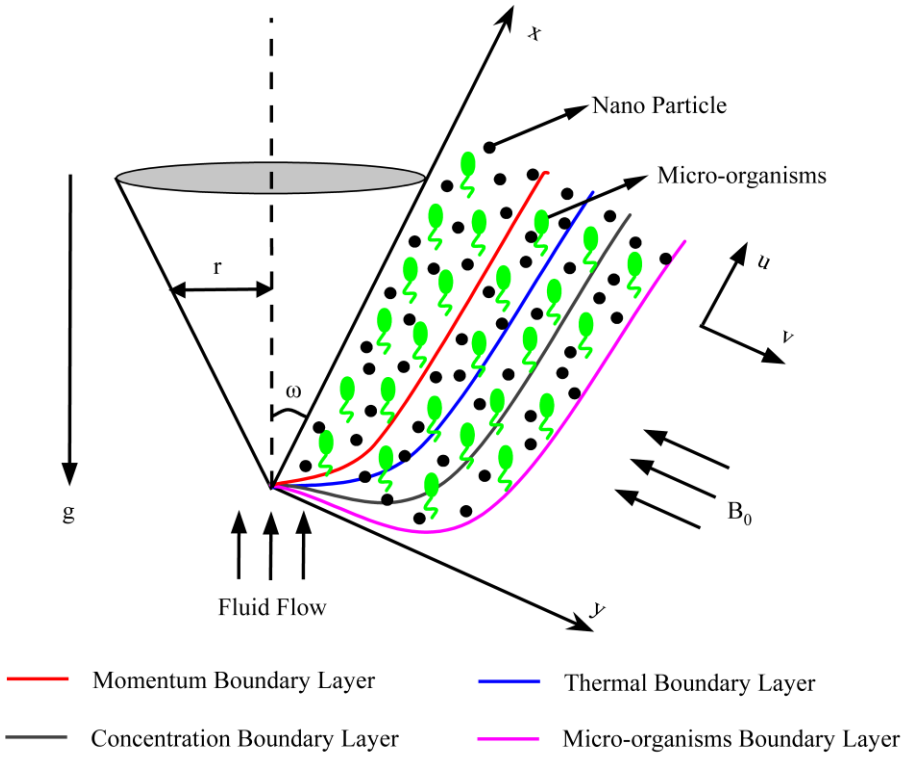

Figure 1. Physical model

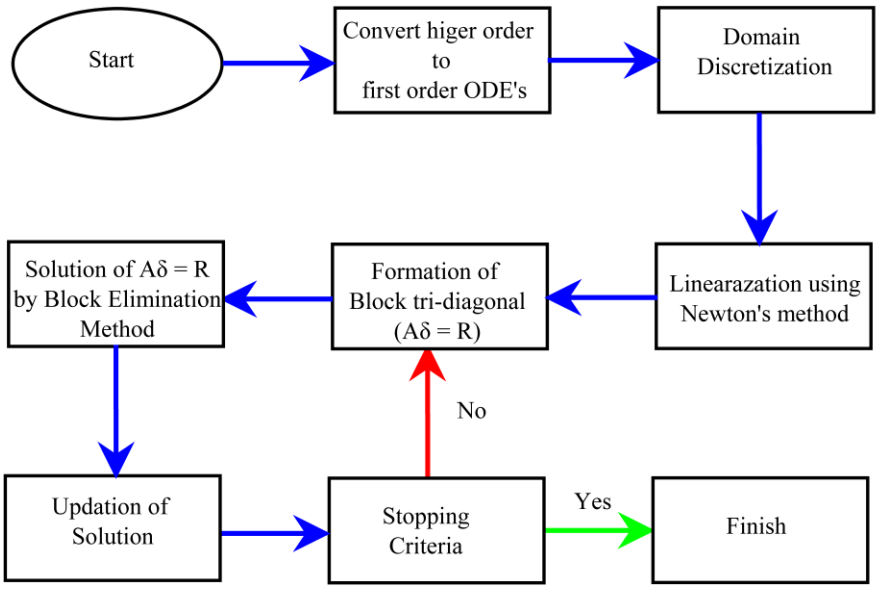

Figure 2. Flowchart illustrating the Keller box approach

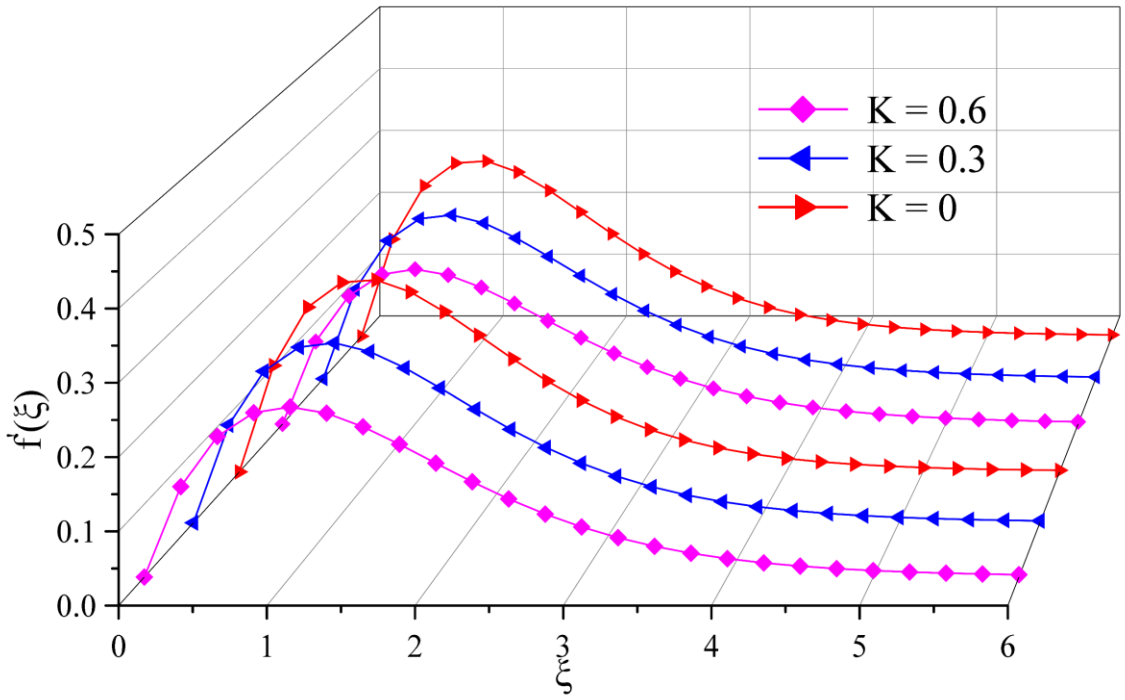

Figure 3. Role of K on velocity

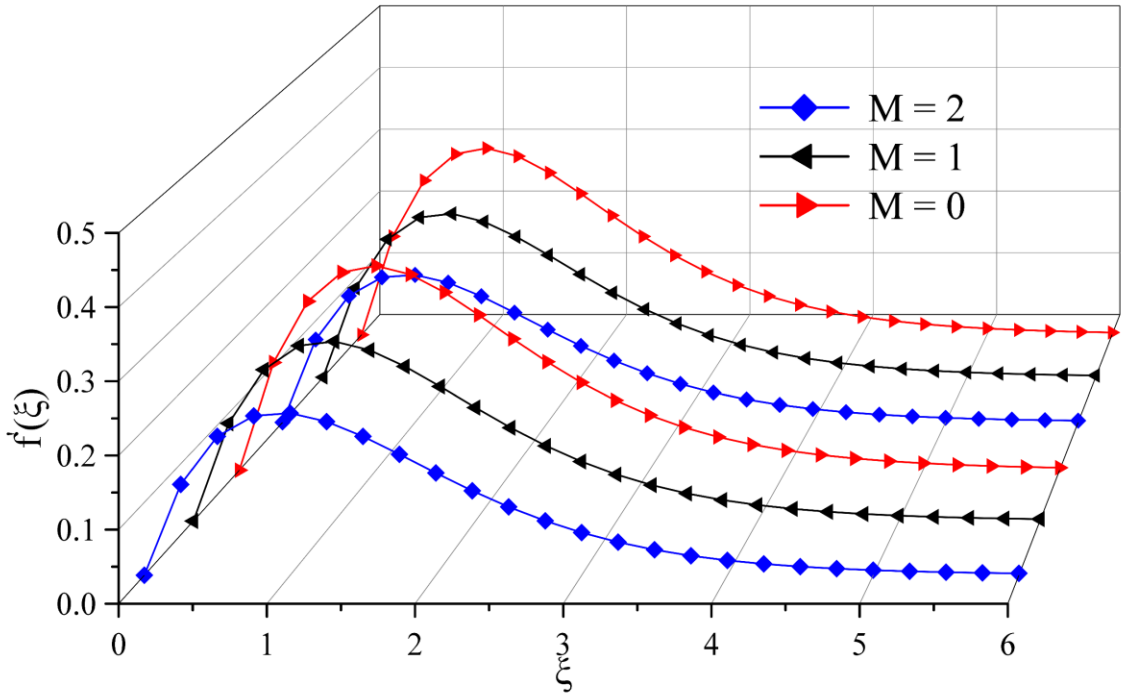

Figure 4. Role of M on velocity

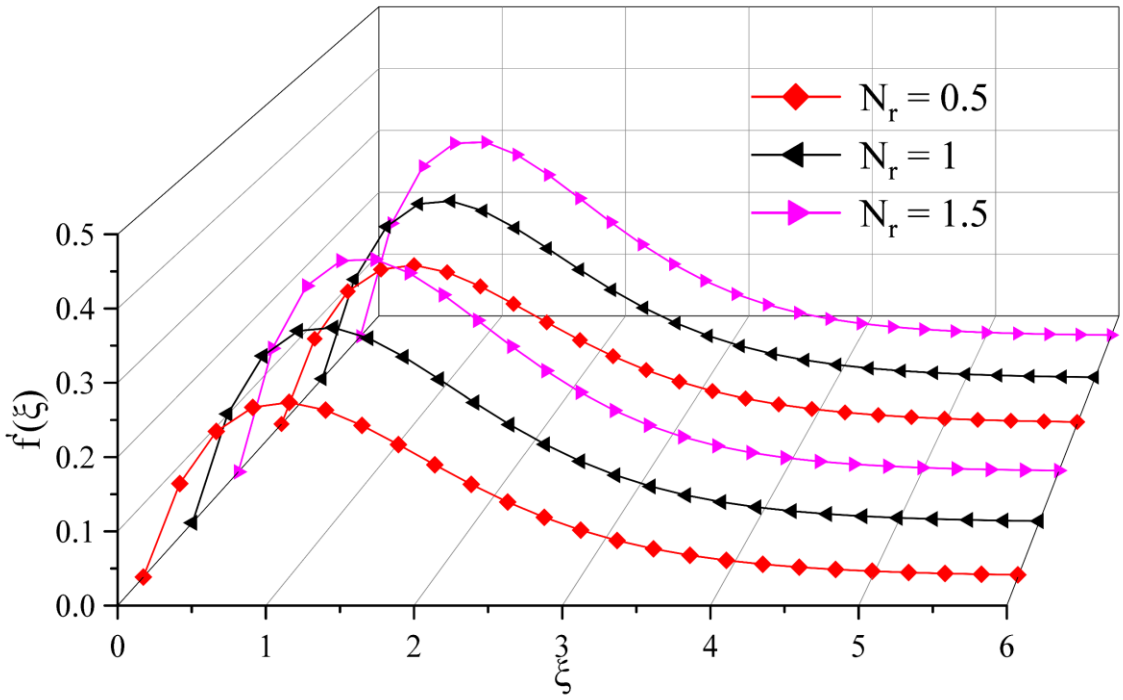

Figure 5. Role of N_r on velocity

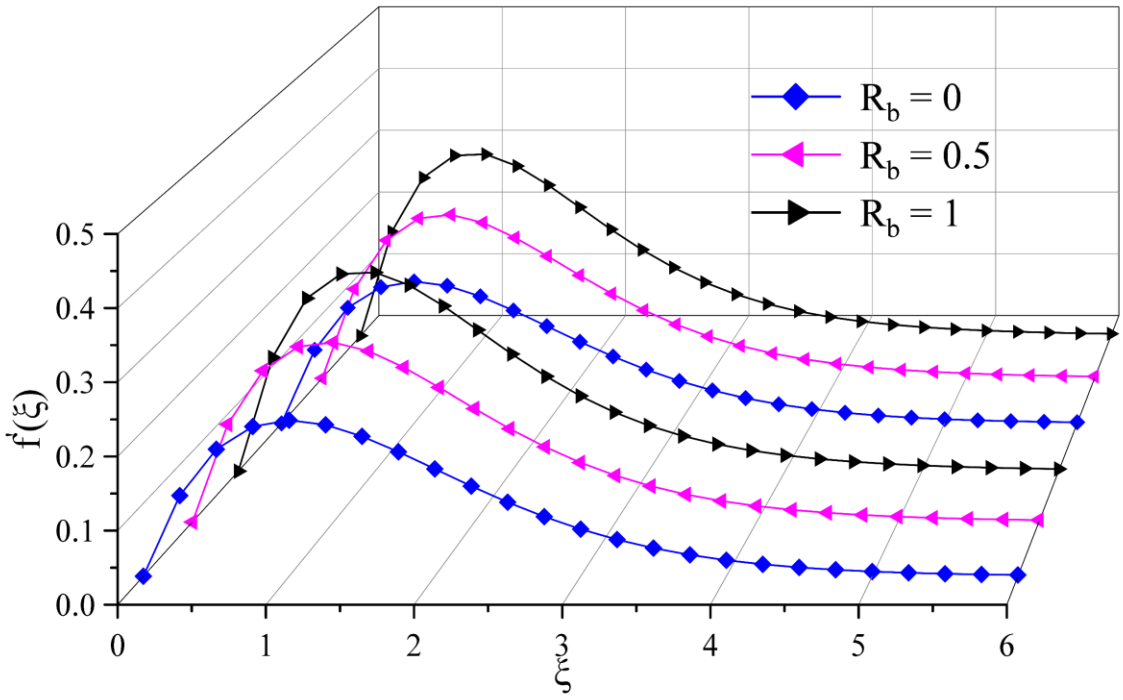

Figure 6. Role of R_b on velocity

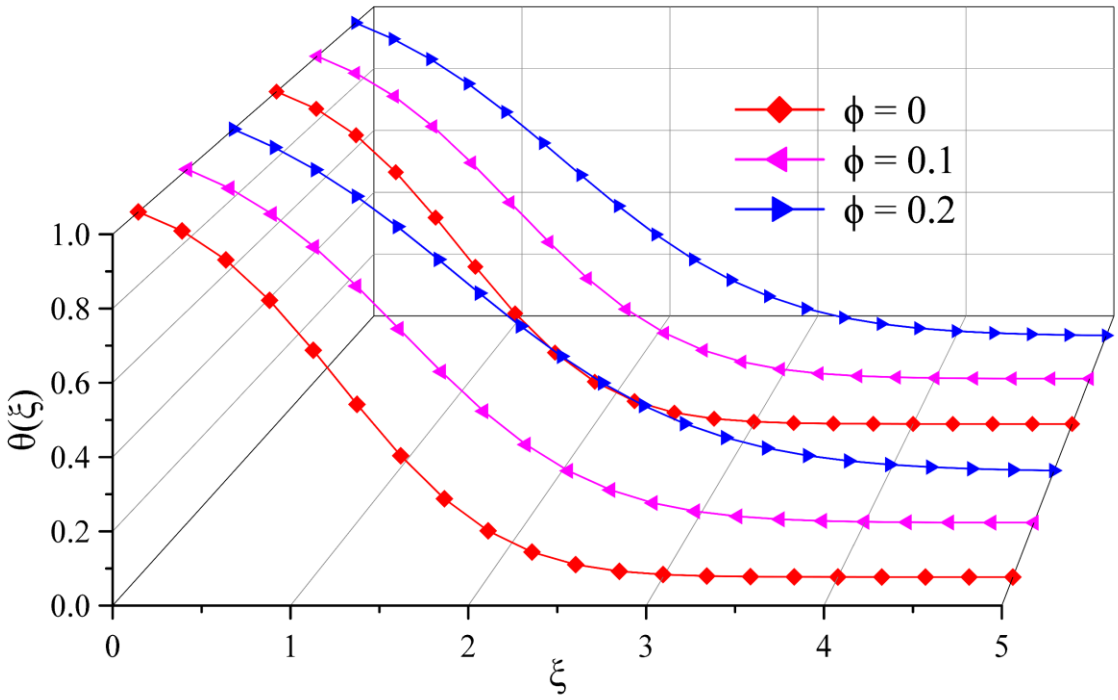

Figure 7. Role of ϕ on temperature

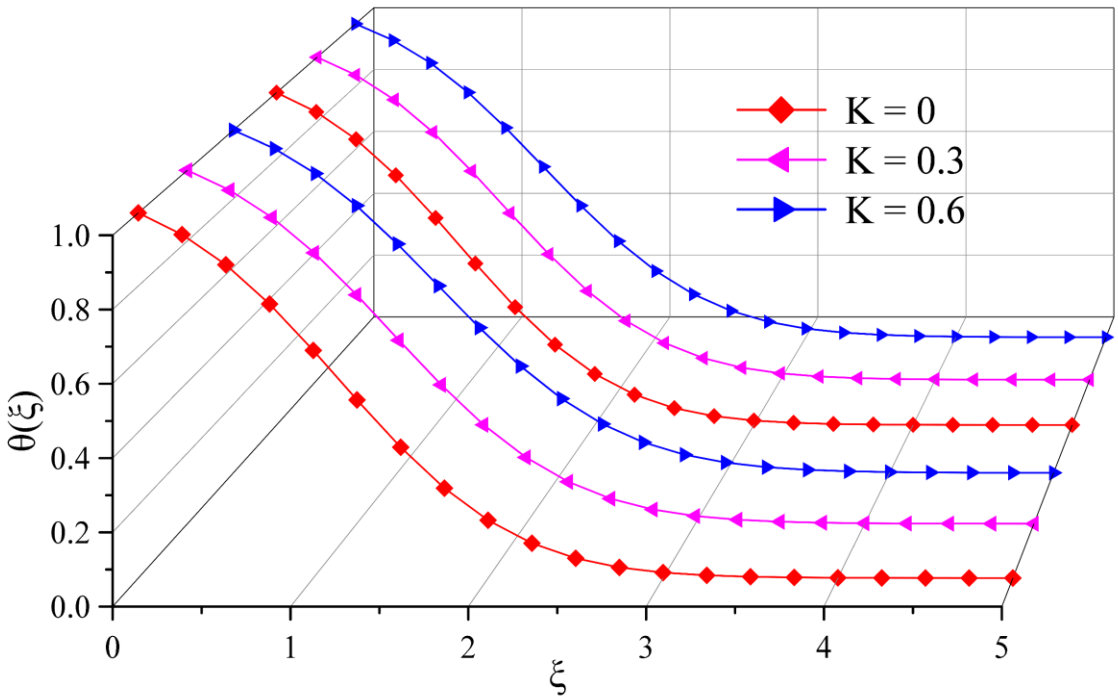

Figure 8. Role of K on temperature

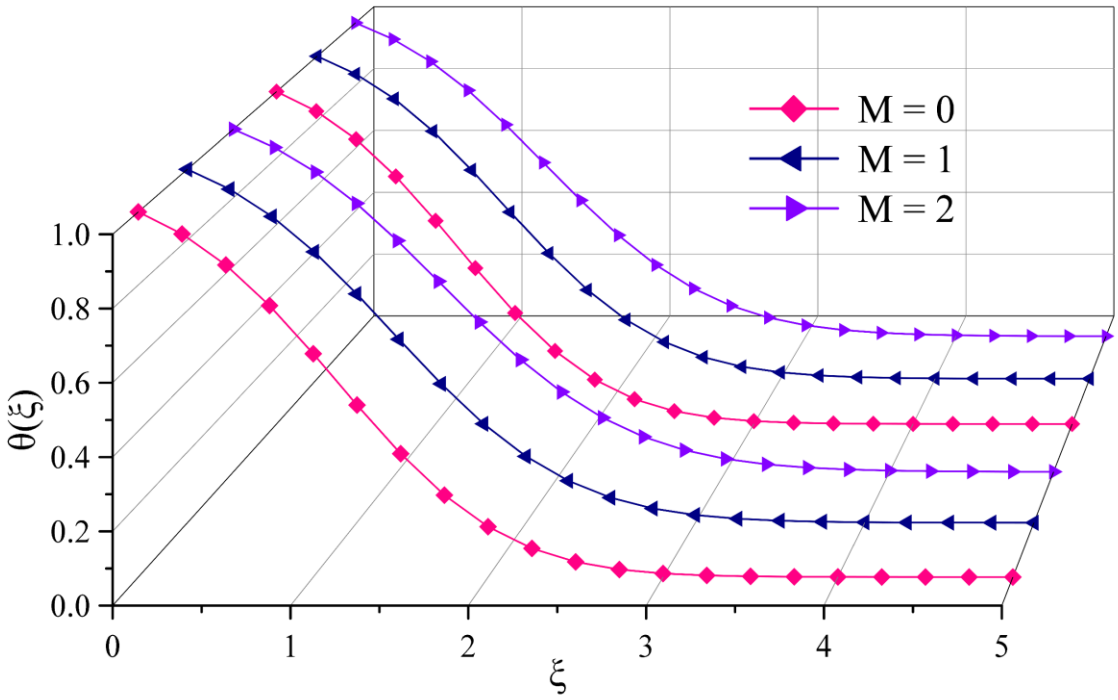

Figure 9. Role of M on temperature

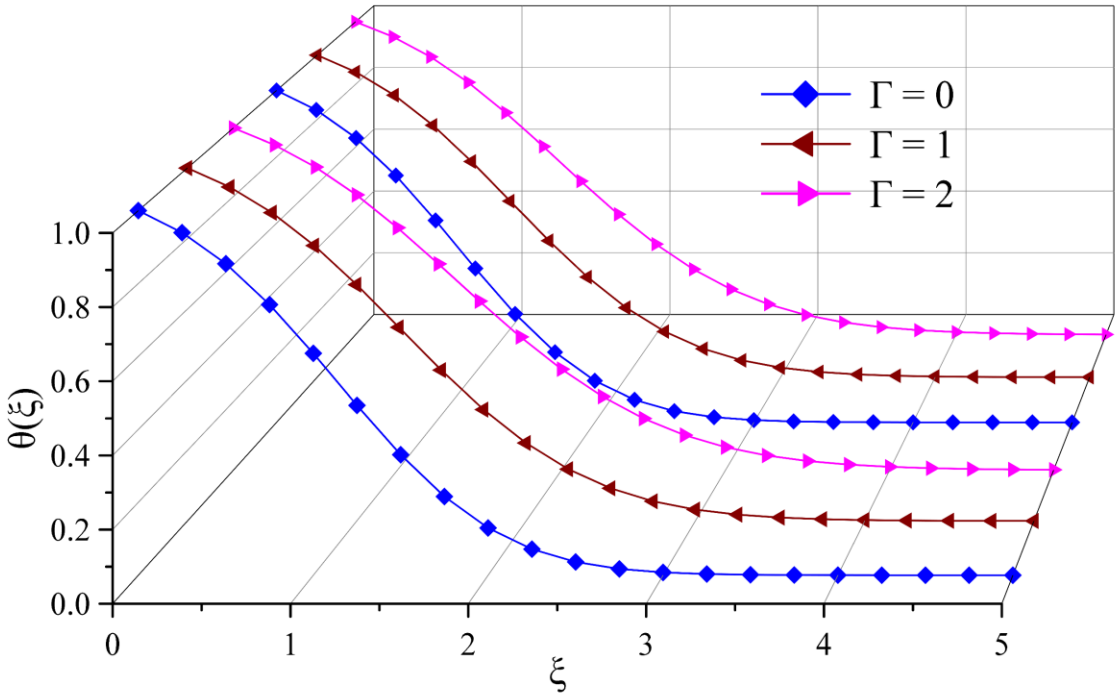

Figure 10. Role of Γ on temperature

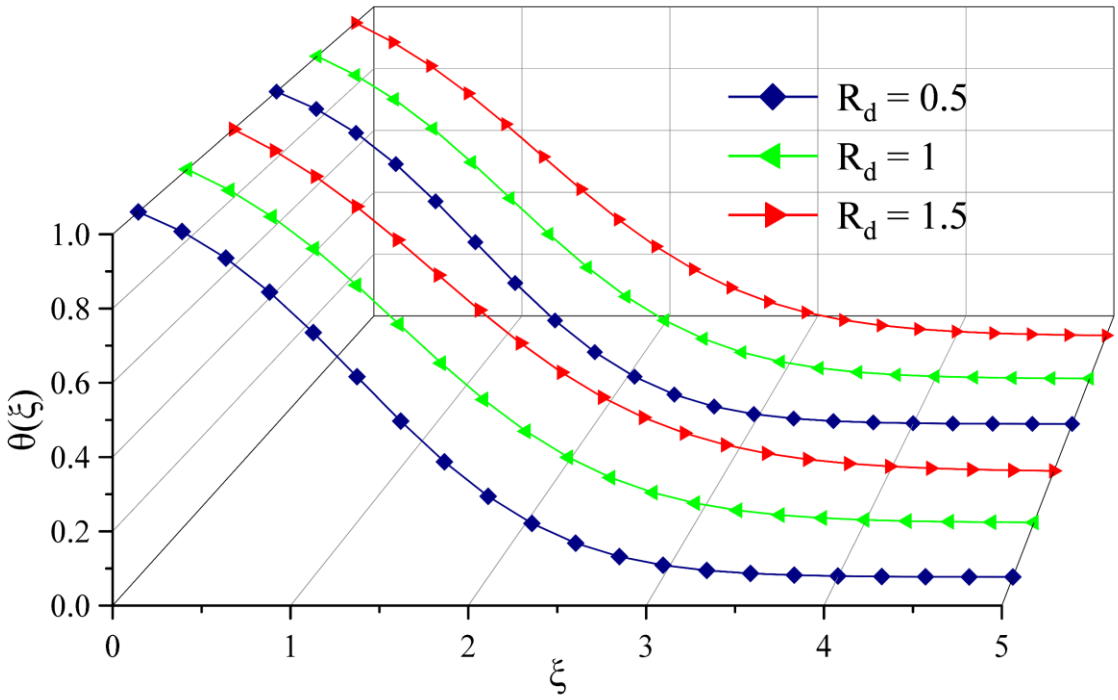

Figure 11. Role of R_d on temperature

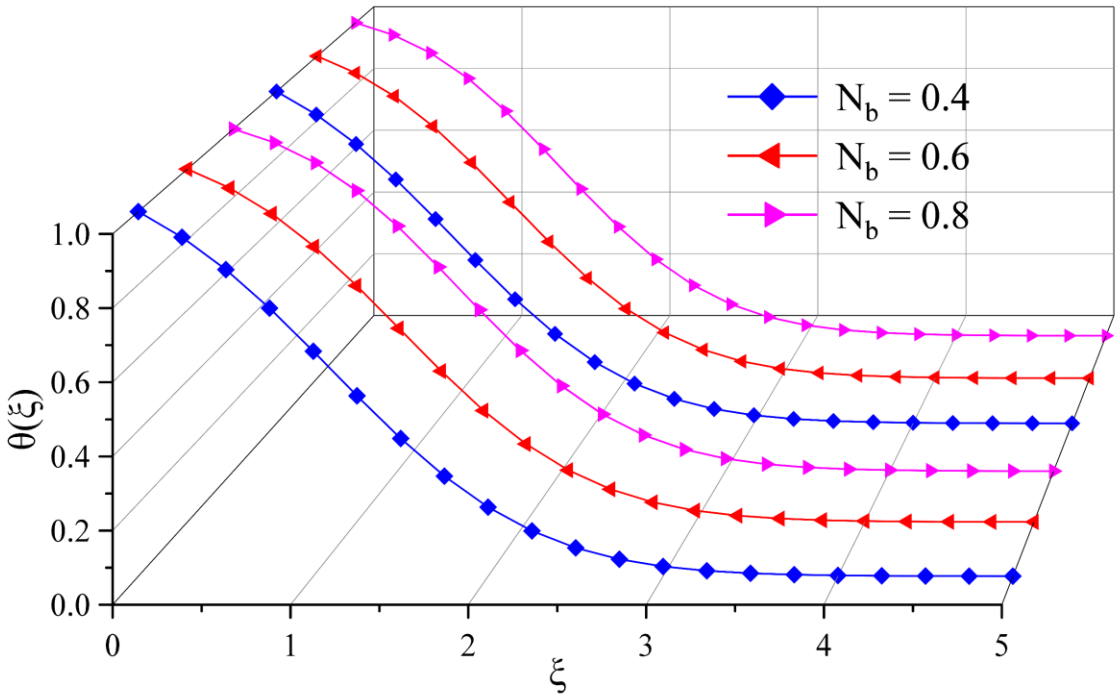

Figure 12. Role of N_b on temperature

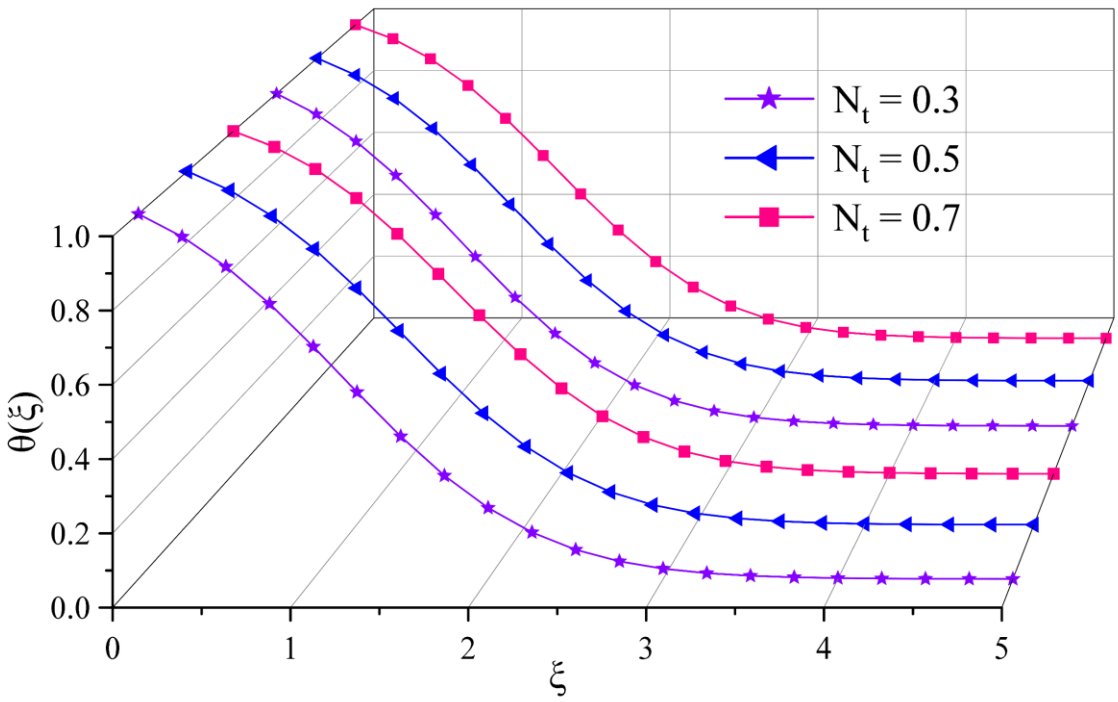

Figure 13. Role of N_t on temperature

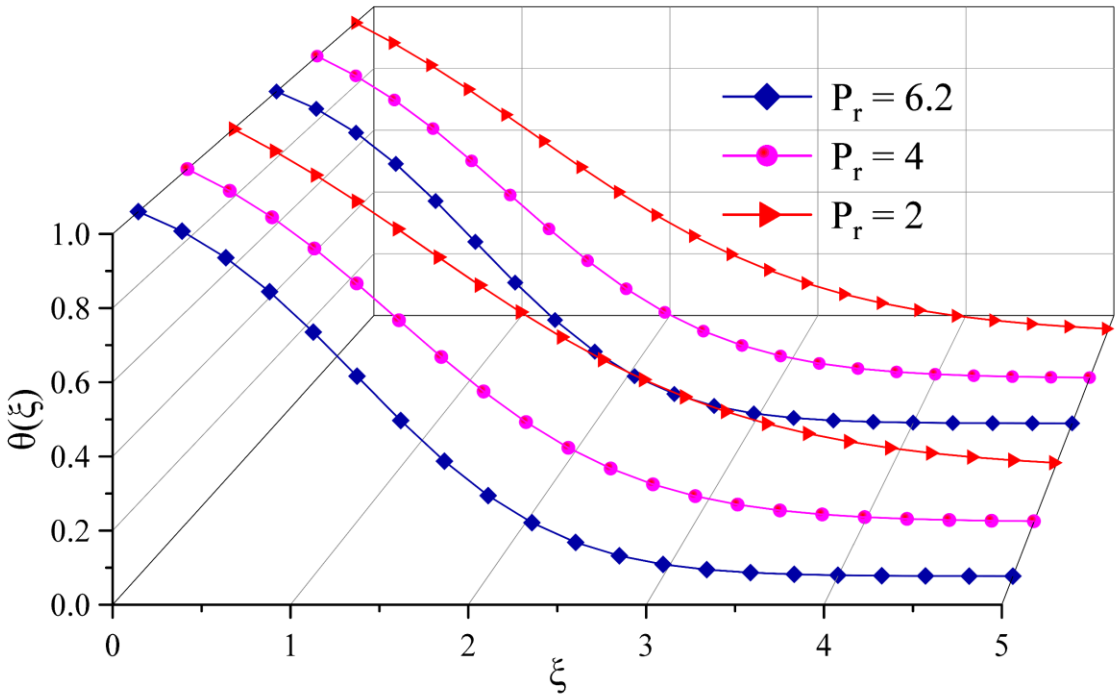

Figure 14. Role of P_r on temperature

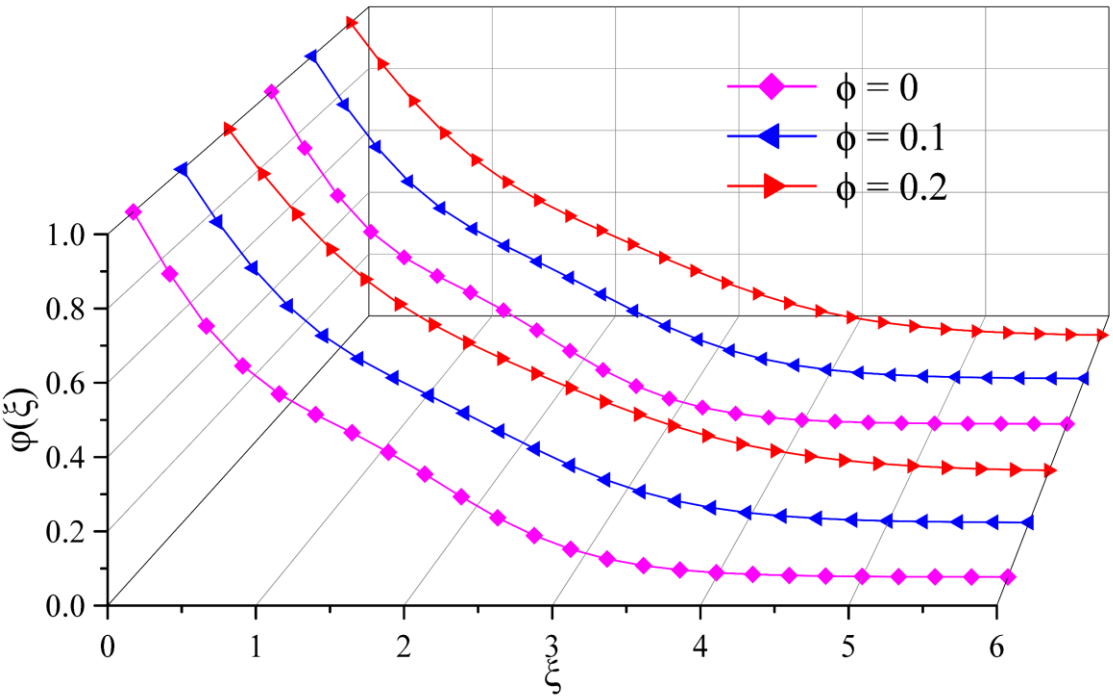

Figure 15. Role of ϕ on concentration

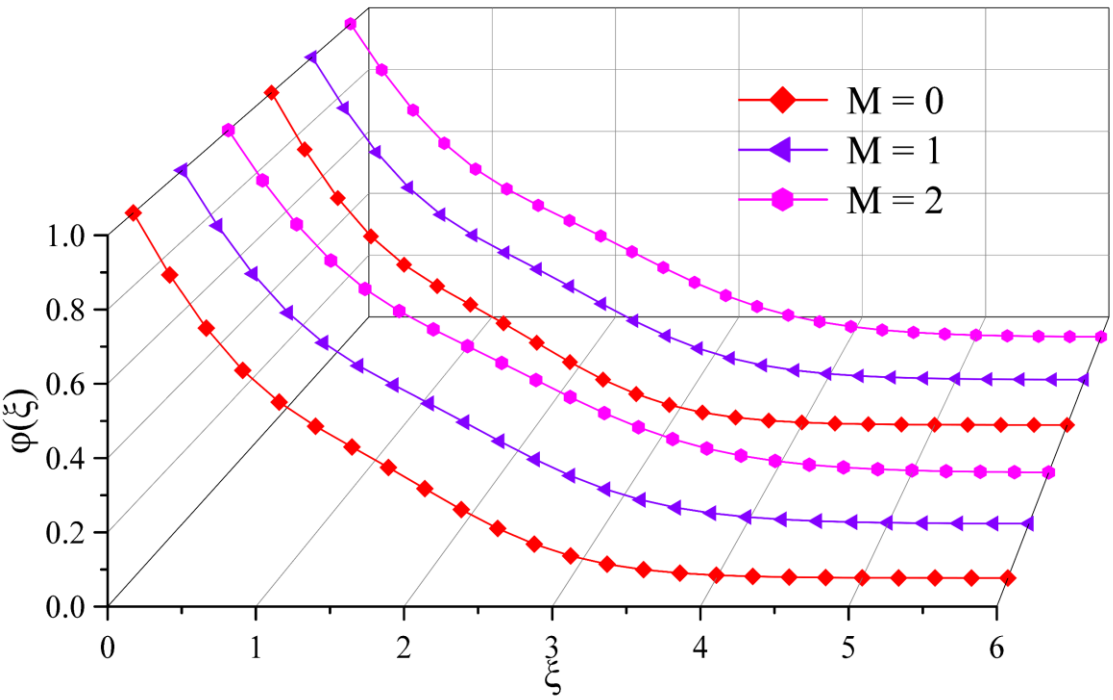

Figure 16. Role of M on concentration

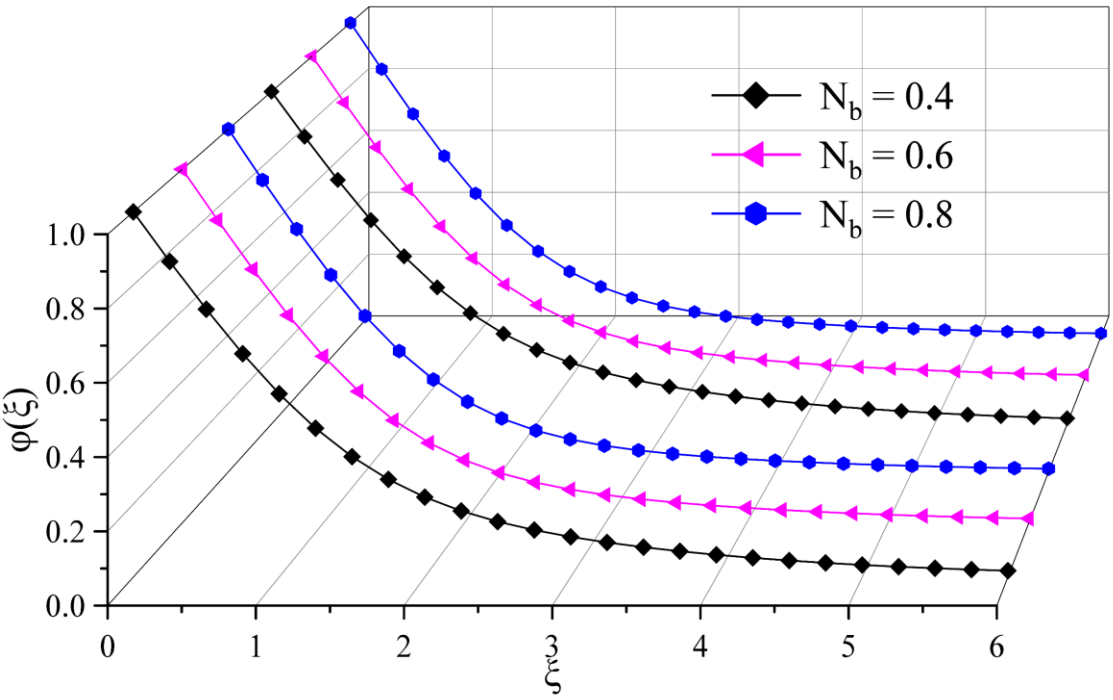

Figure 17. Role of N_b on concentration

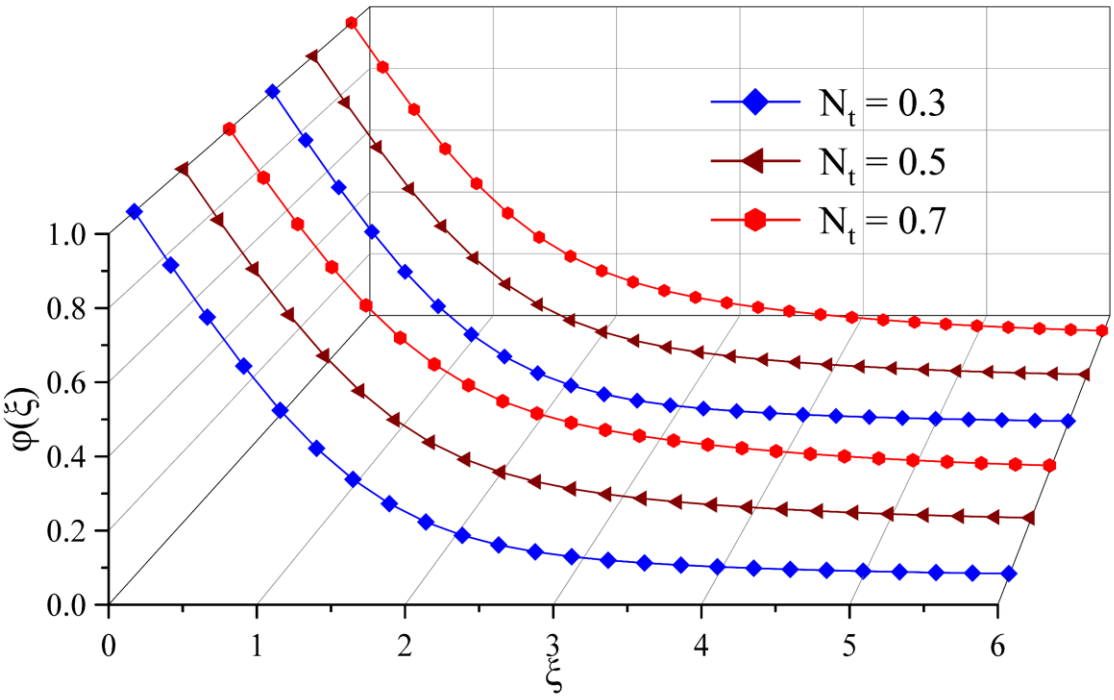

Figure 18. Role of N_t on concentration

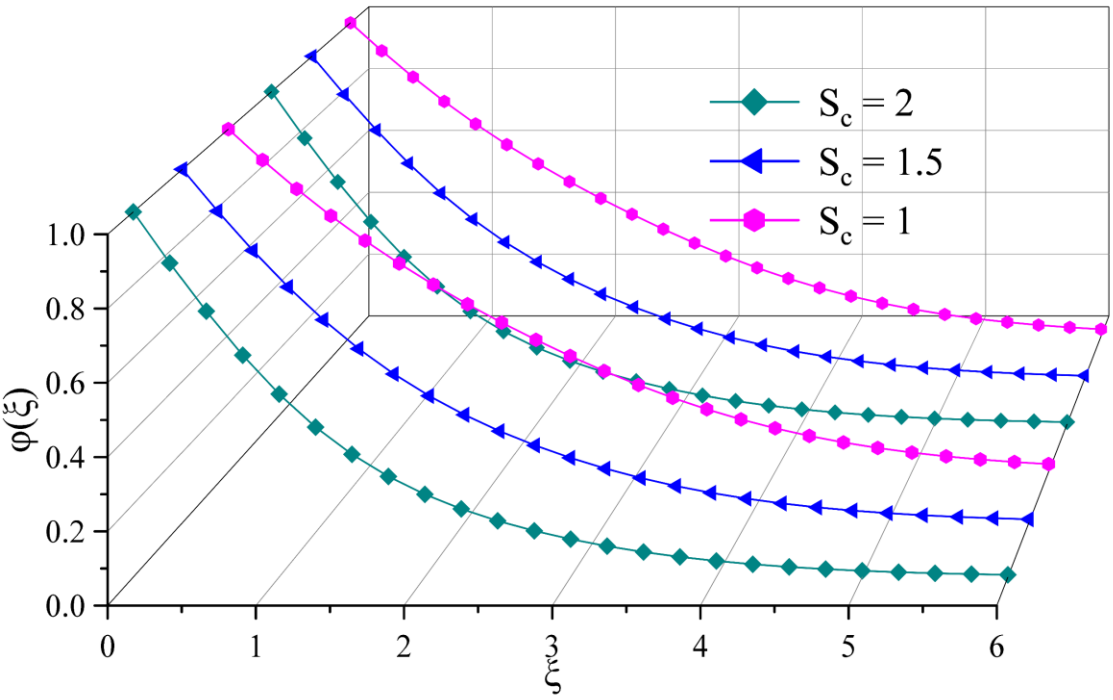

Figure 19. Role of S_c on concentration

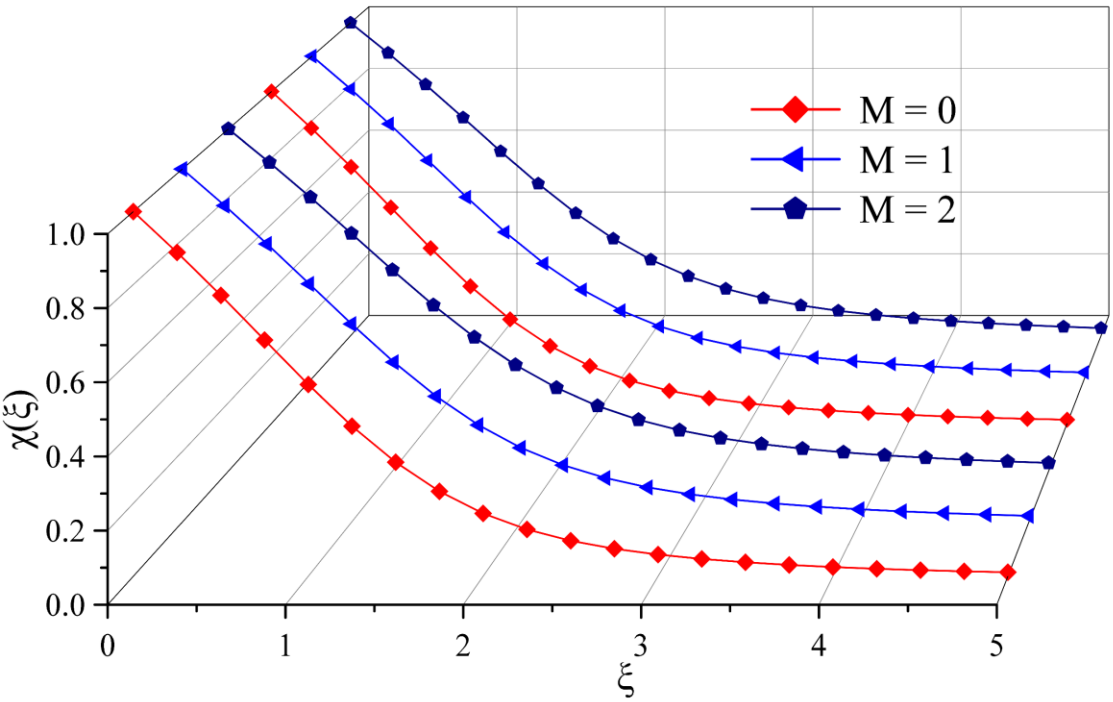

Figure 20. Role of M on microorganism

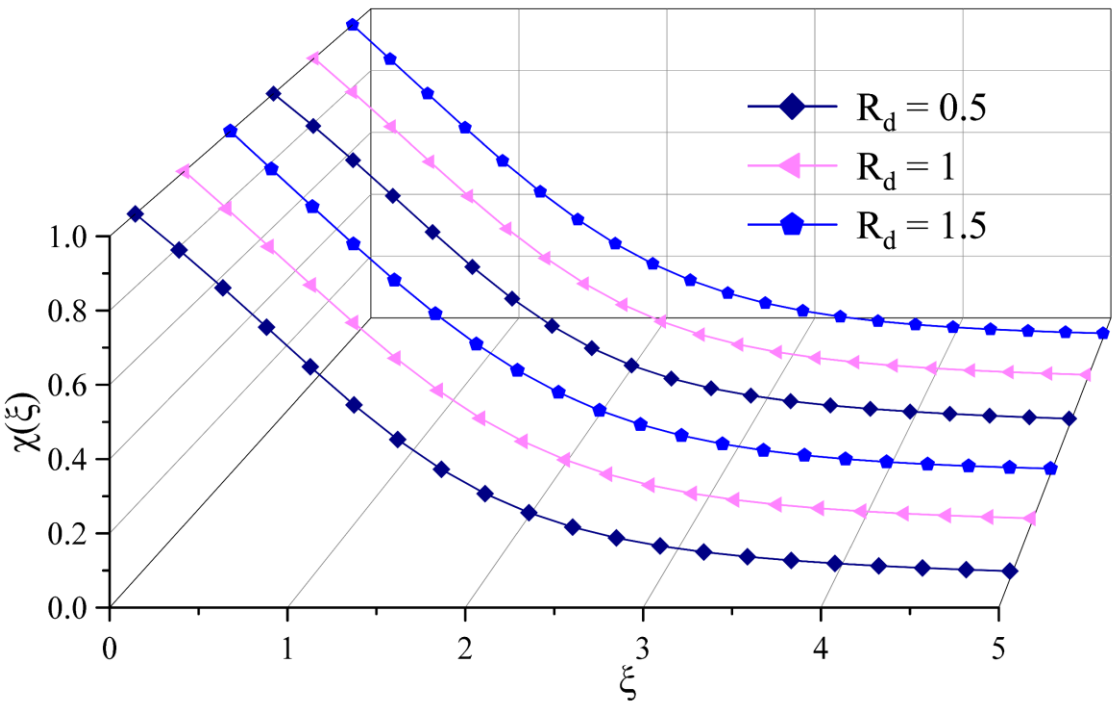

Figure 21. Role of R_d on microorganism

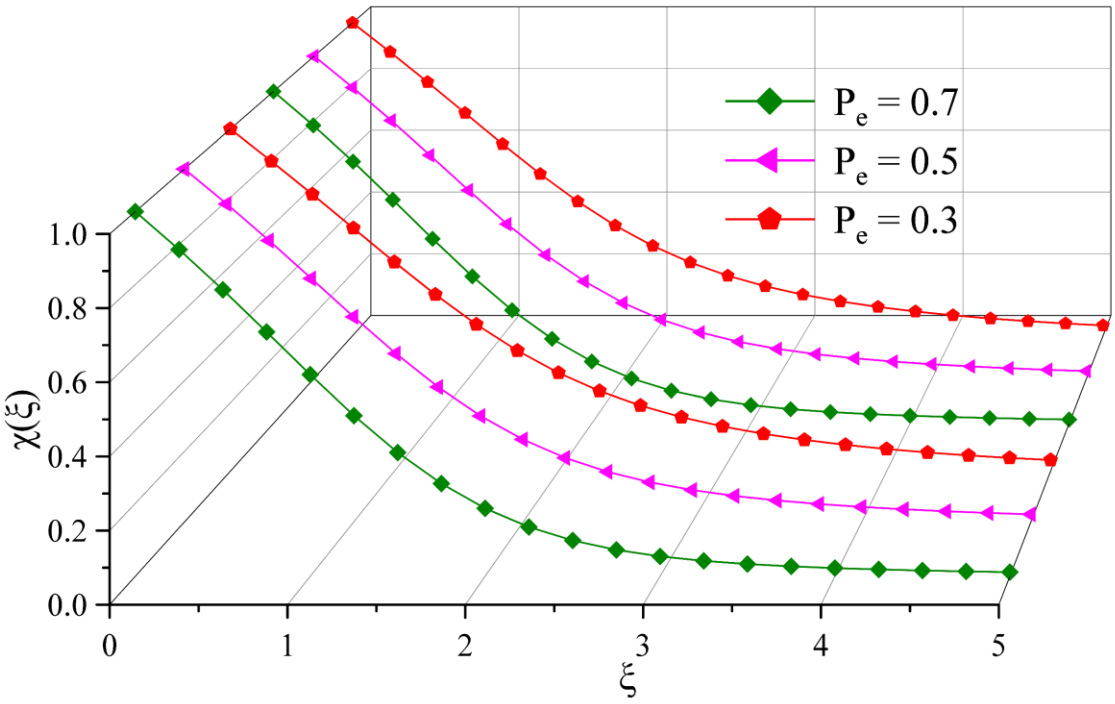

Figure 22. Role of P_e on microorganism

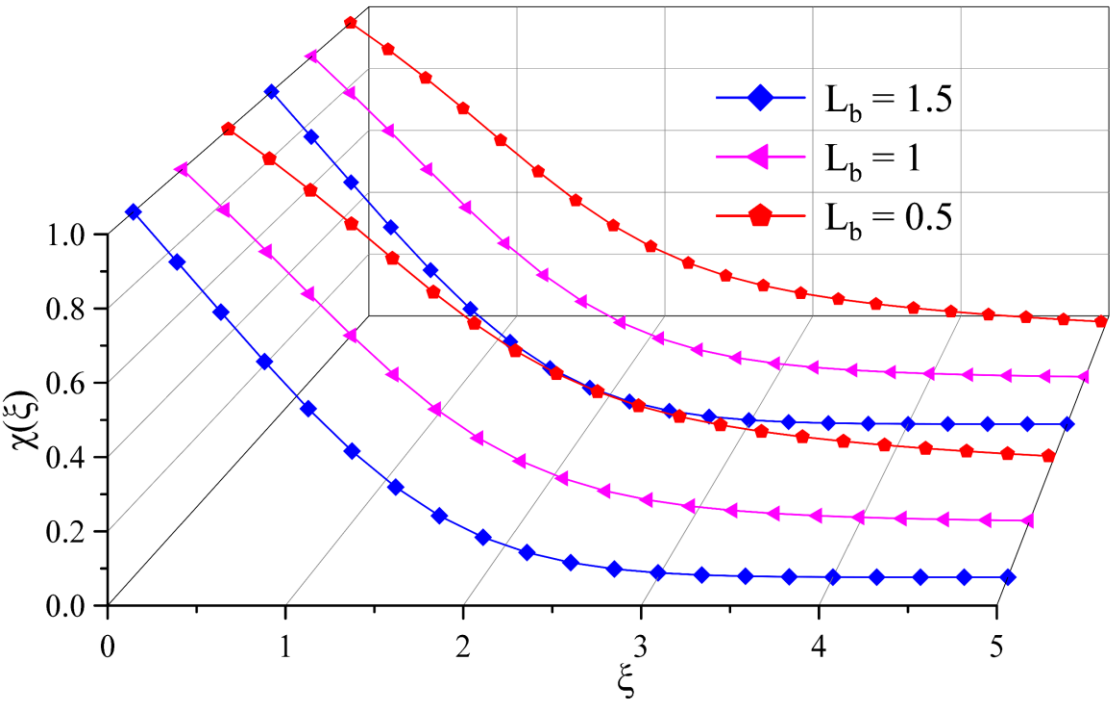

Figure 23. Role of L_b on microorganism

List of Tables:

Table 1. Water and nanoparticle thermo-physical characteristics

Fluid	ρ	Cp	k	$\beta \times 10^{-5}$
H_2O	997.1	4179	0.613	21
Al_2O_3	3970	765	40	0.85
TiO_2	4250	686.2	8.9538	0.9

Table 2. Comparison between the findings of previous research and the results obtained in the current study. Maintaining the values in the manner $\phi = 0$, $N_r = 1$, $R_b = 0$, $R_d = 0$, $L_b = 0$, $P_e = 0$, $S_c = 1$, $N_1 = 2$.

			Macharla Jayachandra Babu et al. [16]			**present**		
M	Γ	K	C_f	$-[d\theta/d\xi]_{(\xi=0)}$	$-[d\varphi/d\xi]_{(\xi=0)}$	C_f	$-[d\theta/d\xi]_{(\xi=0)}$	$-[d\varphi/d\xi]_{(\xi=0)}$
0.8	1	0.2	1.152229	0.468076	0.313377	1.1522301	0.4680765	0.3133778
1.2	1	0.2	1.095732	0.45870	0.304023	1.0957330	0.4587002	0.3040231
1.6	1	0.2	1.046513	0.450237	0.295629	1.0465135	0.4502373	0.2956291
0.6	1	0.2	1.183798	0.473153	0.318462	1.1837981	0.4731528	0.3184632
0.6	2	0.2	1.026461	0.446405	0.291817	1.0264612	0.4464051	0.2918169
0.6	3	0.2	0.916951	0.426244	0.272151	0.9169511	0.4262443	0.2721505

0.6	1	0	1.181208	0.471739	0.315835	1.1812087	0.4717391	0.3158354
0.6	1	0.2	1.183798	0.473153	0.318462	1.1837979	0.4731534	0.3184607
0.6	1	0.4	1.178133	0.474832	0.320356	1.1781333	0.4748321	0.3203559

Table 3. Friction between cone and fluid (local skin friction (C_f))

ϕ	K	N_1	M	Γ	N_r	R_b	Al_2O_3	TiO_2
0.1	0.4	2	1	1	0.7	0.5	1.154429	1.153637
0.2							1.110168	1.108599
0.3							1.051933	1.049746
0.1	**0.2**	2	1	1	0.7	0.5	1.127593	1.126763
	0.4						1.154429	1.153637
	0.6						1.180415	1.179651
0.1	0.4	**1**	1	1	0.7	0.5	1.164001	1.163187
		2					1.154429	1.153637
		3					1.143167	1.142403
0.1	0.4	2	**1**	1	0.7	0.5	1.154429	1.153637
			1.5				1.101276	1.100679
			2				1.054712	1.054251
0.1	0.4	2	1	**1**	0.7	0.5	1.154429	1.153637
				2			0.999335	0.999015
				3			0.892880	0.892747
0.1	0.4	2	1	1	**0.5**	0.5	1.063940	1.063086
					0.7		1.154429	1.153637
					0.9		1.242752	1.242020
0.1	0.4	2	1	1	0.7	**0.3**	1.071047	1.070253
						0.5	1.154429	1.153637
						0.7	1.235708	1.234916

Table 4. Heat transfer rate (local Nusselt number ($-\theta'(0)$))

ϕ	K	N_1	R_d	N_b	N_t	Al_2O_3	TiO_2
0.1	0.4	2	0.5	0.6	0.5	0.526801	0.511669
0.2						0.571109	0.534307
0.3						0.639877	0.564096
0.1	**0.2**	2	0.5	0.6	0.5	0.541704	0.526116
	0.4					0.526801	0.511669
	0.6					0.512903	0.498194
0.1	0.4	**1**	0.5	0.6	0.5	0.525401	0.510298
		2				0.526801	0.511669
		3				0.528436	0.513271
0.1	0.4	2	**0.5**	0.6	0.5	0.526801	0.511669
			0.7			0.571032	0.556652
			1			0.632651	0.619161
0.1	0.4	2	0.5	**0.4**	0.5	0.565652	0.550418
				0.6		0.526801	0.511669
				0.8		0.494021	0.478951
0.1	0.4	2	0.5	0.6	**0.3**	0.537124	0.522214
					0.5	0.526801	0.511669
					0.7	0.516002	0.500665

Table 5. Mass transfer rate (local sherwood number ($-\varphi'(0)$))

ϕ	K	N_1	S_c	N_b	N_t	R_d	Al_2O_3	TiO_2
0.1	0.4	2	0.8	0.6	0.5	0.5	0.352367	0.350603
0.2							0.330864	0.326975
0.3							0.307079	0.300666
0.1	**0.2**	2	0.8	0.6	0.5	0.5	0.362266	0.360401

	0.4						0.352367	0.350603
	0.6						0.343125	0.341448
0.1	0.4	**1**	0.8	0.6	0.5	0.5	0.351438	0.349690
		2					0.352367	0.350603
		3					0.353454	0.351670
0.1	0.4	2	**0.4**	0.6	0.5	0.5	0.199311	0.196820
			0.8				0.352367	0.350603
			1.2				0.452915	0.451576
0.1	0.4	2	0.8	**0.4**	0.5	0.5	0.304858	0.302090
				0.6			0.352367	0.350603
				0.8			0.376244	0.374976
0.1	0.4	2	0.8	0.6	**0.3**	0.5	0.374930	0.373310
					0.5		0.352367	0.350603
					0.7		0.333399	0.331661
0.1	0.4	2	0.8	0.3	0.5	**0.5**	0.352367	0.350603
						0.7	0.357956	0.356342
						1	0.365432	0.364023

Table 6. local micro-organisms density number ($-\chi'(0)$)

ϕ	K	N_1	L_b	P_e	σ	R_b	Al_2O_3	TiO_2
0.1	0.4	2	0.7	0.5	0.4	0.5	0.473103	0.472378
0.2							0.428844	0.427338
0.3							0.381928	0.379607
0.1	**0.2**	2	0.7	0.5	0.4	0.5	0.487127	0.486335
	0.4						0.473103	0.472378
	0.6						0.460080	0.459413
0.1	0.4	**1**	0.7	0.5	0.4	0.5	0.471527	0.470816

		2					0.473103	0.472378
		3					0.474954	0.474213
0.1	0.4	2	**0.5**	0.5	0.4	0.5	0.421873	0.421058
			0.7				0.473103	0.472378
			1				0.536449	0.535826
0.1	0.4	2	0.7	**0.3**	0.4	0.5	0.446455	0.445704
				0.5			0.473103	0.472378
				0.7			0.498625	0.497939
0.1	0.4	2	0.7	0.5	**0.3**	0.5	0.465017	0.464300
					0.4		0.473103	0.472378
					0.5		0.481177	0.480443
0.1	0.4	2	0.7	0.5	0.4	**0.3**	0.460514	0.459789
						0.5	0.473103	0.472378
						0.7	0.485108	0.484382